Homeodomain protein Sxi1α independently controls cell-cell fusion and gene expression during sexual reproduction in *Cryptococcus deneoformans*

Jun Huang, Anna E. Lehmann, Patricia P. Peterson, Ziyan Xu, Liping Xiong, Sheng Sun, and Joseph Heitman*

Department of Molecular Genetics and Microbiology, Duke University Medical Center, Durham, NC 27710, USA

* Corresponding author: Joseph Heitman
Email: heitm001@duke.edu

Keywords: Homeodomain protein; Sexual reproduction; Cell fusion; Transcriptional regulation.

Abstract

Sex-specific homeodomain (HD) proteins are key regulators of cell identity and sexual development in fungi, typically functioning as heterodimers to govern transcription. In the human fungal pathogens *Cryptococcus neoformans* and *Cryptococcus deneoformans*, the HD proteins Sxi1α and Sxi2**a** (Sex-inducer 1α and 2**a**) have been characterized as interacting components that play critical roles in sexual development during α x **a** sexual reproduction. α cells are the predominant mating type in natural populations of *Cryptococcus*, and unisexual (same-sex) mating can also occur in certain genetic backgrounds. The roles of Sxi1α and Sxi2**a** in unisexual reproduction are not fully understood. To elucidate the functions of Sxi1α and Sxi2**a**, we first applied AlphaFold3 prediction, which identified potential heterodimeric and homodimeric complexes. Formation of a Sxi2**a** homodimer was then experimentally validated through yeast two-hybrid assays. We subsequently deleted *SXI1*α and *SXI2***a** in the hyper-filamentous self-fertile *C. deneoformans* strains XL280α and XL280**a**. Disruption of these genes did not result in noticeable defects in vegetative growth, virulence-associated traits, colony morphology, sporulation, or competitive fitness during unisexual crosses. Interestingly, both bilateral (mutant x mutant) and unilateral (mutant x wildtype) crosses involving the *sxi1*αΔ mutant significantly increased α-α cell fusion efficiency, suggesting a previously unrecognized inhibitory role for Sxi1α in regulating same-sex cell fusion. Consistently, genes encoding mating pheromones and the α-pheromone receptor Ste3 were upregulated in the *sxi1*αΔ fusion assays. Transcriptomic analysis of *sxi1*αΔ and *sxi2***a**Δ mutants led to the identification of unique subsets of genes negatively regulated by each transcription factor during unisexual reproduction. Additionally, α x **a** crosses between null mutants of *sxi1*αΔ and *sxi2***a**Δ revealed differential regulation of mating-type (*MAT*) loci genes dependent only on Sxi1α or Sxi2**a**. Together, our findings reveal a novel role for Sxi1α in governing cell fusion and demonstrate that Sxi1α and Sxi2**a** have distinct transcriptional control during unisexual and α x **a** sexual reproduction, potentially exerting opposing regulation of sex-specific *MAT* genes.

Author Summary

Analogous to processes observed in many eukaryotic organisms, fungal sexual reproduction reshuffles genetic material, producing novel genetic variants with increased fitness and/or adaptive potential. The human fungal pathogen *Cryptococcus deneoformans* is widespread in the environment and can cause severe infections in immunocompromised individuals. Sexual reproduction in this species occurs between cells of either opposite mating types (α x **a** mating) or the same mating type (α x α and **a** x **a** unisexual reproduction). The mating type-specific homeodomain transcription factors Sxi1α and Sxi2**a** are known to form a complex that broadly controls sexual development following α and **a** cell fusion. Here, we find that Sxi1α inhibits cell-cell fusion during unisexual reproduction, while its partner, Sxi2**a**, shows only limited inhibition in certain genetic contexts. Further, we show that Sxi1α and Sxi2**a** regulate transcription of distinct gene sets during both α x **a** and unisexual reproduction, including many within the mating-type (*MAT*) loci, often in opposing manners. Together, these findings reveal that Sxi1α and Sxi2**a** function both cooperatively and independently, thereby allowing for a more flexible and finely-tuned mating control system than previously recognized, providing insight into how this organism generates genetic variation and adapts to changing environments.

84 **Introduction**

85 Sexual reproduction is a key process in eukaryotic organisms, promoting genetic diversity and
86 facilitating adaptation to changing environments. In fungi, this process is controlled by the mating-type
87 (*MAT*) locus, a specific genomic region containing genes required for successful mating [1]. Among these
88 genes, pheromone and pheromone receptors (P/R) are involved in signal transduction and recognition
89 between mating partners, and homeodomain (HD) transcription factors act as master regulators that control
90 the expression of genes necessary for sexual development [2,3]. In the model yeast *Saccharomyces*
91 *cerevisiae*, **a**1 and α2 are well-characterized HD proteins, forming **a**1-α2 heterodimers that bind DNA
92 cooperatively to repress transcription of cell type-specific genes [4,5]. Unlike **a**1, which has no known role
93 in the absence of α2, α2 can form homodimers, as well as partner with the Mcm1 cofactor to repress **a**-
94 specific genes in α and **a**/α cells [6–9]. In the corn smut fungus *Ustilago maydis*, the HD proteins bWest
95 (bW) and bEast (bE) dimerize to regulate fungal morphological switching and interactions with the plant
96 host [10–13]. Similarly, sexual development in the mushroom *Coprinus cinereus* requires the physical
97 interaction of two HD proteins, HD1 and HD2 [14]. Conserved and convergent functionality of HD
98 transcription factors across diverse fungi illustrates their centrality to species survival and proliferation.

99 The human fungal pathogen *Cryptococcus neoformans* is the predominant cause of cryptococcal
100 meningoencephalitis worldwide, whereas its sister species *C. deneoformans* displays a more
101 geographically restricted distribution and is more frequently encountered in certain regions, particularly in
102 Europe [15–17]. Interestingly, in *C. neoformans* and *C. deneoformans*, the *P/R* and *HD* genes as well as
103 additional genes reside in a relatively large (>100 kb) *MAT* locus [2,17–19]. In addition to its direct role in
104 α x **a** sexual reproduction, the *MAT* locus is associated with several other functions in *Cryptococcus*,
105 including virulence and uniparental mitochondrial inheritance (mito-UPI), in which mitochondrial DNA is
106 predominantly inherited from the *MAT***a** parent after α x **a** sexual reproduction [20,21]. We previously
107 identified the *Cryptococcus* sex-specific HD proteins Sxi1α (Sex inducer 1α) and Sxi2**a** (Sex inducer 2**a**),
108 which heterodimerize upon α-**a** cell fusion and are involved in key development processes including cell
109 identity determination, sexual development, and mito-UPI [2,21,21–25]. Our group and others have
110 identified several Sxi1α-Sxi2**a** targets for which proper temporal expression is essential for sexual
111 development. For example, *CPR2* (*Cryptococcus* pheromone receptor 2) governs α-**a** cell fusion, and *CLP1*

112 (clampless 1) is required for post-cell fusion dikaryotic filament formation [26–29]. Beyond these well-
113 characterized targets, the identification of several hundred Sxi1α/Sxi2**a**-bound promoter elements in *C.*
114 *neoformans* suggests that this complex has a much broader regulatory role in sexual development [29].

115 In addition to α x **a** sexual reproduction, unisexual reproduction can also occur between partners
116 of the same mating type (mainly α x α) in *C. neoformans* and *C. deneoformans* [30–32]. In natural
117 *Cryptococcus* populations, *MAT*α isolates are predominant among both clinical and environmental samples,
118 suggesting that α x **a** heterothallic sexual reproduction is infrequent [20,33], even though population
119 genomics studies have shown that recombination is occurring among *Cryptococcus* isolates in nature
120 [33,34]. This strong bias in *MAT* locus distribution may, at least in part, be explained by the occurrence of
121 unisexual reproduction, which enables genetic recombination and propagation in the absence of a
122 compatible mating partner [30,35,36]. As key sex-specific transcriptional regulators, the roles of Sxi1α and
123 Sxi2**a** in unisexual reproduction and their transcriptional targets remain to be elucidated.

124 In this study, we sought to determine whether Sxi1α and Sxi2**a** are involved in same-sex mating in
125 *C. deneoformans*. AlphaFold3 structural prediction suggested that Sxi1α and Sxi2**a** may form both
126 heterodimeric and homodimeric complexes, and the formation of the Sxi2**a** homodimer was further
127 confirmed by yeast two-hybrid assays. Taking advantage of the hyper-filamentous *C. deneoformans*
128 congenic isolates XL280α and XL280**a** [37], along with a CRISPR/Cas9-based gene editing system [38,39],
129 we deleted *SXI1*α and *SXI2***a** in XL280α and XL280**a**, respectively. Consistent with previous results, we
130 found that *SXI1*α and *SXI2***a** are dispensable for vegetative growth and multiple *in vitro* virulence-relevant
131 traits, including thermotolerance at 37°C, polysaccharide capsule formation, and melanin production.
132 Interestingly, compared to fusion between two wildtype *MAT*α strains, we observed a significant increase
133 in α-α fusion efficiency when Sxi1α was deleted in one or both *MAT*α strains, which is accompanied by
134 significant upregulation of genes encoding mating pheromones and the α-pheromone receptor *STE3*.
135 Similarly, increased **a**-**a** fusion was observed when Sxi2**a** was deleted in one of the two *MAT***a** strains, but
136 not when Sxi2 was absent in both strains, pointing to a previously unrecognized inhibitory function of Sxi1α
137 in same-sex cell fusion. No apparent defects in colony morphology, hyphal development, basidium
138 formation, sporulation, spore germination, or competitive fitness were detected in *sxi1*αΔ or *sxi2***a**Δ mutants
139 during unisexual reproduction. Transcriptomic analysis revealed distinct sets of genes for which expression

differences are regulated only by Sxi1α, independent of its canonical interacting partner Sxi2**a**. The Sxi1α-dependent gene set in the unisexual crosses is markedly smaller and has limited overlap with that in α x **a** crosses. These observations support the hypothesis that Sxi1α has distinct functions during α x **a** and α x α sexual reproduction that is independent of Sxi2**a**.

Our results suggest a novel function of Sxi1α in regulating cell-cell fusion, expanding our understanding of how HD proteins contribute to fungal sexual reproduction. Additionally, we show that Sxi1α and Sxi2**a** have transcriptional regulatory effects both dependently and independently of one another. These findings, combined with our structural predictions and yeast two-hybrid-validated Sxi2**a** homodimer, support the hypothesis that Sxi1α and Sxi2**a** may have distinct functions independently of their usual HD partner, analogous to α2 in budding yeast. Overall, these findings further our understanding of how sexual reproduction is regulated in this important human fungal pathogen and reveal important differences in Sxi1α and Sxi2**a** transcription factor activity between unisexual and α x **a** sexual reproduction.

Results

Sxi1α and Sxi2a are predicted to form a heterodimer

To study the impact of the homeodomain proteins Sxi1α and Sxi2**a** on unisexual reproduction in *Cryptococcus*, we selected to study XL280α and XL280**a**, a pair of congenic *C. deneoformans* strains that are well-known for their ability to undergo unisexual reproduction involving robust self-filamentation and sporulation [30,37]. Sxi1α and Sxi2**a** are conserved between *C. neoformans* and *C. deneoformans*, and homeodomain (Pfam:00046) or homeobox KN domains (from **KN**OX family transcription factors, Pfam:PF05920) were found within the sequences via an NCBI conserved domain search (Fig 1A). Both domains are structurally related, sharing DNA-binding functions through a helix-turn-helix motif, consistent with potential functional relevance in governing gene expression. Consistent with our previous report with yeast two-hybrid analysis [2,22], a heterodimer between Sxi1α and Sxi2**a** was predicted by AlphaFold3 protein-protein complex prediction (Fig 1B). Pairwise structural alignments between the predicted Sxi1α-Sxi2**a** heterodimer and the crystal structure of the *S. cerevisiae* **a**1-α2 heterodimer [40] revealed robust structural similarity between the two homeodomain complexes with an RMSD value of 0.561 angstroms between 49 pruned atom pairs (Fig 1C). Similarly, the Sxi1α-Sxi2**a** heterodimer exhibited high structural similarity to the AlphaFold3-predicted bW-bE heterodimer from the corn smut fungus *Ustilago maydis*, with a RMSD of 1.069 angstroms across 40 pruned atom pairs. Interestingly, the HD2 proteins [2], represented by Sxi2**a**, **a**1, and bW, superimpose closely, reflecting strong evolutionary conservation. In contrast, greater structural divergence was observed among the HD1 proteins, including Sxi1α, α2, and bE, consistent with their roles in conferring regulatory specificity. Together, these comparisons support a conserved functional framework in which HD2 provides a structurally stable DNA-binding platform, while HD1 contributes specificity to transcriptional regulation, with heterodimer formation serving as a central regulatory module in mating control [41].

Previous studies showed that, in addition to forming a heterodimer with **a**1, *S. cerevisiae* α2 forms a homodimer to repress **a**-specific genes [9]. To benchmark the reliability of our structural predictions, we applied AlphaFold3 to the well-characterized yeast **a**1 and α2. Consistent with experimental evidence, AlphaFold3 predicted robust homodimer formation for α2 but not for **a**1, supporting the validity of this approach for distinguishing biologically relevant homodimerization events (S1 Fig). Using this validated

180 framework, we next asked whether Sxi1α and Sxi2**a** might also form homodimers, we utilized AlphaFold3
181 to model Sxi1α-Sxi1α and Sxi2**a**-Sxi2**a** interactions. The predictions indicated potential low-confidence
182 homodimer formation for Sxi1α-Sxi1α (ipTM = 0.14, pTM = 0.23) and Sxi2**a**-Sxi2**a** (ipTM = 0.20, pTM =
183 0.24) (Fig 1D). These low interface and predicted TM-scores suggest weak or unstable interactions. It is
184 also possible that any homodimerization could involve additional interacting partner(s) that are not yet
185 known, or that Sxi1α and Sxi2**a** could have independent roles analogous in function but distinct in structure
186 from those observed in ascomycetous yeast.

187 To determine whether Sxi1α or Sxi2**a** could form homodimers, we performed yeast two-hybrid (Y2H)
188 analyses with Gal4 DNA-binding domain (GBD) and transcriptional activation domain (GAD) fusion
189 constructs (Fig 1E). Because homeodomain transcription factors frequently function as dimers, we
190 specifically tested whether either protein could self-associate in this heterologous system. We also included
191 the putative *C. deneoformans* ortholog of Mcm1, a transcription factor involved in the pheromone response
192 pathway in other fungi including *S. cerevisiae*, where it interacts with the homeodomain protein α2 and
193 transcription factor Ste12 to regulate mating-specific gene expression [42,43]. We identified *C.*
194 *deneoformans* Mcm1 (CNN00060) and *C. neoformans* Mcm1 (CNAG_07924) as orthologs of *S. cerevisiae*
195 Mcm1 through reciprocal BLASTp searches. Our AlphaFold3 prediction and alignment suggest a
196 conserved structural organization between the *S. cerevisiae* α2-Mcm1 [44] and the *C. deneoformans* Sxi1α-
197 Mcm1(CNN00060) (S2 Fig), and we hypothesize that Mcm1 could similarly interact with Sxi1α or Sxi2**a** in
198 *Cryptococcus*. Thus, we tested all possible pairwise interactions between Sxi1α, Sxi2**a**, and Mcm1.

199 Plasmids encoding the fusion proteins were transformed into the Y2H reporter strains Y2HGold
200 and Y187. Following mating of the two strains, diploids were selected and assayed for Gal4-dependent
201 activation of *ADE2*, *HIS3*, and *lacZ* reporter genes. In a previous study, full-length Sxi2**a** fused to GBD was
202 shown to auto-activate reporter gene expression [2]. Consistent with this observation, auto-activation was
203 also detected in our assays for both Sxi2**a** and Mcm1 (S3 Fig). To avoid false-positive interactions resulting
204 from auto-activation, we instead analyzed a truncated form of Sxi2**a** (Sxi2**a**N), containing only the N-
205 terminal region and the homeodomain (HD), for interaction testing. A robust protein-protein interaction was
206 detected between Sxi2**a**N and full-length Sxi2**a**, supporting the AlphaFold-predicted model of a Sxi2**a**
207 homodimer (Fig 1E). In contrast, we did not detect evidence for Sxi1α homodimerization, or between Mcm1

208 and Sxi1α or Sxi2**a** in this assay (S4 Fig). While these results suggest that such interactions are either
209 weak or absent in this context, we cannot exclude the possibility that dimerization or complex formation
210 may occur *in vivo* and require post-translational modifications or additional binding partners not
211 recapitulated in the yeast two-hybrid system.
212
213 **Sxi1α and Sxi2a are dispensable for *in vitro* growth and virulence-related traits**
214 To further characterize the phenotypic impact of Sxi1α and Sxi2**a**, we generated *SXI1*α and *SXI2***a**
215 null mutants in XL280α and XL280**a**, respectively, with a CRISPR/Cas9-based strategy following the
216 previously-established TRACE electroporation protocol [38,39]. Multiple independent drug-resistant
217 transformants [four for XL280α *sxi1*αΔ::*NAT* and two for XL280**a** *sxi2***a**Δ::*NEO*] were constructed and
218 confirmed with correct genotypes as deletion mutants based on 5' junction, 3' junction, and internal ORF-
219 specific PCR analysis (Fig 2A). Mapping of reads generated from Illumina whole-genome sequencing
220 further confirmed the complete deletion of the genes in all four *sxi1*αΔ mutants and one of the two *sxi2***a**Δ
221 mutants, and a partial gene deletion in the other *sxi2***a**Δ mutant (Fig 2B and S5 Fig). In some of the mutants,
222 elevated read-depth was observed in the flanking regions employed for homologous recombination during
223 gene deletion (Fig 2B and S5 Fig). This could indicate potential concatemeric or ectopic insertion [45] of
224 the resistance cassette (Fig 2B and S5 Fig). For the partial deletion mutant XL280**a** *sxi2***a**Δ#6, the deletion
225 occurred between the 5' microhomology sequence and the second gRNA targeting site, instead of at the 3'
226 microhomology sequence (S5 Fig). This pattern is consistent with a hybrid integration event in which NHEJ
227 and HR [46] occurred on opposite sides of the construct. Importantly, no sequencing reads mapped to the
228 N-terminal region of the gene that encompasses the conserved homeodomain (S5 Fig). Therefore, Sxi2**a**
229 is functionally disrupted in this mutant, and the strain was retained for subsequent analyses.
230 We next performed competition assays to assess the impact of Sxi1α and Sxi2**a** on fungal fitness
231 during vegetative growth. Equal amounts of mutant and wildtype cells were inoculated in liquid YPD
232 medium and cultured for 48 hours at 30°C. Samples were collected at 0h, 24h, and 48h to assess
233 population dynamics. In all cases, the *sxi1*αΔ and *sxi2***a**Δ strains maintained similar proportions to wildtype
234 during co-culture, indicating that the mutations confer no detectable fitness defect (Fig 2C). Additionally,
235 we characterized the contributions of Sxi1α and Sxi2**a** to several major virulence traits: thermotolerance at

236 37°C, capsule formation, and melanin production. Consistent with our previous reports in *C. neoformans*
237 [23], none of the *sxi1*α*Δ* or *sxi2***a***Δ C. deneoformans* deletion strains displayed fitness differences compared
238 to the XL280 wildtype strains in these assays (Fig 2D-2F). Taken together, these results indicate that the
239 loss of *SXI1*α and *SXI2***a** does not affect the fitness of the XL280 strain during vegetative growth and has
240 no detectable impact on virulence-related traits under the conditions tested.
241
242 **Sxi1α and Sxi2a are dispensable for morphology, sporulation, and cell viability during unisexual**
243 **reproduction**
244 We next investigated whether Sxi1α and Sxi2**a** are involved in unisexual reproduction in the XL280
245 background. When grown on mating- and selfing-inducing MS solid medium [47] as solo-cultures, all of the
246 tested *sxi1*α*Δ* and *sxi2***a***Δ* mutants produce elongated hyphae, basidia, and basidiospore chains at levels
247 similar to the XL280 wildtype controls (Fig 3A and 3B). No discernable differences in the basidia and
248 basidiospores were observed by scanning electron microscope (SEM) (Fig 3C). Thus, the deletion of *SXI1*α
249 and *SXI2***a** did not affect unisexual reproduction morphologically in the XL280 background. Additionally, we
250 collected random meiotic basidiospores by microdissection to test the effect of Sxi1α and Sxi2**a** on spore
251 germination rates and cell viability and found no significant difference in germination rates between spores
252 produced by the *sxi1*α*Δ* mutants and XL280α (p-values: 0.682 (*sxi1*α*Δ*#4 vs XL280α) and 0.125 (*sxi1*α*Δ*#5
253 vs XL280α), Welch's t-test), as well as between spores produced by the *sxi2***a***Δ* mutants and XL280**a** (p-
254 values: 0.591 (*sxi2***a***Δ*#6 vs XL280**a**:) and 0.750 (*sxi2***a***Δ* #7 vs XL280**a**), Welch's t-test) (Fig 3D). No
255 significant difference in spore germination rate was observed between the congenic wildtype strains
256 XL280α and XL280a (p-value: 0.0856, Welch's t-test) (Fig 3D).
257 We previously observed that strains capable of undergoing unisexual reproduction outcompete
258 mutants with unisexual reproduction defects under mating-inducing conditions, attributable to enhanced
259 hyphal growth and sporulation [48]. To assess the effects of *SXI1*α and *SXI2***a** deletion on this metric of
260 unisexual reproduction efficiency, for each deletion strain we mixed equal numbers of cells from the mutant
261 (containing a dominant drug-resistant marker) and its wildtype control strain (sensitive to drug), and spotted
262 the mixture on MS medium to induce unisexual reproduction. After robust sporulation was observed (10
263 days post plating), we dissected two populations: 1) random basidiospores from the periphery where

264 sporulation occurs, and 2) the center of the spot where cells remain mostly as yeast (Fig 3E, left panel).
265 Germinated dissected spores/yeast cells were transferred onto YPD plates containing selective drug (NAT
266 or NEO) to determine which strain in the mixture they originated from. For both *sxi1*α*Δ* and *sxi2***a***Δ*, the
267 ratios between mutant and wildtype among the basidiospores at the periphery were similar to those among
268 the yeast cells at the center (spores/yeast, p-values: 0.5398275 (*sxi1*α*Δ*) and 0.379667 (*sxi2***a***Δ*), paired t-
269 test), indicating the loss of Sxi1α and Sxi2**a** does not affect competitive fitness during unisexual reproduction
270 (Fig 3E, right panel).

271 The DNA-binding protein Mcm1 functions as a central transcriptional co-regulator of mating type
272 homeodomain proteins during sexual development in budding yeast [43,44]. Because *Cryptococcus* Sxi1α
273 and Sxi2**a** have structural and functional commonalities with *S. cerevisiae* α2 and **a**1, we questioned
274 whether an analogous co-factor may exist in *Cryptococcus*. We first examined whether deletion of *MCM1*
275 affects unisexual reproduction by generating *mcm1*Δ mutants in the XL280 background (S6 Fig) and tested
276 their self-fertility under mating-inducing conditions. Deletion of *MCM1* did not result in obvious defects in
277 unisexual mating morphology in either XL280α or XL280**a** (S7 Fig). To test for potential synthetic effects
278 between *MCM1* and *SXI1*α or *SXI*2**a**, we constructed *sxi1*α*Δ mcm1*Δ and *sxi2*a*Δ mcm1*Δ double mutants
279 (S6 Fig). No clear unisexual mating morphology defects were observed in these strains (S7 Fig).
280 Interestingly, it appears that all of the engineered strains containing *mcm1*Δ deletion displayed an increased
281 abundance of yeast cells in the center of mating spots, along with a reduced frequency of basidia bearing
282 robust basidiospore chains (S7 Fig). Additionally, we tested the role of Mcm1 in α x **a** sexual reproduction
283 with an *mcm1*Δ strain derived from the *C. neoformans* H99 transcription factor deletion collection [49].
284 Through mating, we generated the congenic strain KN99**a** *mcm1*Δ. Crosses were performed on MS and
285 V8 (pH=5) media by mating *mcm1*Δ with either wildtype, *sxi1α*Δ, or *sxi2***a***Δ* strains [23]. Consistent with
286 previous observations [2,22], crosses involving *sxi1α*Δ or *sxi2a*Δ exhibited clear mating defects in hyphal
287 development and sporulation (S8 Fig). In contrast, no detectable mating defects were observed in either
288 unilateral or bilateral α x **a** crosses involving *mcm1*Δ (S8 Fig). Collectively, these results indicate that, unlike
289 its essential co-regulatory role in budding yeast, Mcm1 is largely dispensable for both unisexual and α x **a**
290 sexual reproduction in *C. deneoformans* and *C. neoformans.*
291

292 **Sxi1α is critical for unisexual cell-cell fusion**

293 In the presence of a helper strain serving as a pheromone donor, α x α and **a** x **a** outcrossing can
294 be facilitated in *C. deneoformans* in so-called Ménage à trois matings [22,30] (Fig 4A). Previously, our
295 results from α x **a** sexual reproduction suggested that Sxi1α and Sxi2**a** function after cell-cell fusion [2].
296 Although cell-cell fusion is dispensable for solo unisexual reproduction, it may still occur under certain
297 conditions, such as during α x α outcrossing [22,30]. Given the limited understanding of the role of Sxi1α
298 in this context, we sought to determine whether Sxi1α is involved in cell-cell fusion during α x α outcrossing
299 in the presence of a donor strain (JEC20, *MAT***a** *NAT*^{S} *NEO*^{S}). Strains in the XL280α *SXI1*α and *sxi1*αΔ
300 backgrounds that were differentially resistant to *NAT* and *NEO* were used to set up three types of mating:
301 *SXI1*α x *SXI1*α, *SXI1*α x *sxi1*αΔ, and *sxi1*αΔ x *sxi1*αΔ. Equal number of cells of the two strains in each
302 mating were mixed and spotted on V8 agar (pH=7) to induce sexual reproduction. After 72 hours of
303 incubation, cells were collected. The fusion frequency was fewer than 5.04×10^{-8} in two independent sets
304 of the XL280α *NAT* x XL280α *NEO* crosses, with fusion products identified by screening colonies for NAT
305 and NEO resistance. In contrast, significantly higher fusion frequencies were found in *sxi1*αΔ::*NAT* x
306 *sxi1*αΔ::*NEO* (22.5-fold higher than wildtype, frequency: 1.13×10^{-6}, p-value: 0.0013, Welch's t-test) and
307 *sxi1*αΔ::*NAT* x XL280α *NEO* (62.9-fold higher than wildtype, frequency: 3.17×10^{-6}, p-value: 0.0288, Welch's
308 t-test) (Fig 4B). Taken together, these findings demonstrate that cell-cell fusion between *MAT*α cells is
309 significantly increased when *SXI1*α is absent in at least one of the two strains.

310 We then asked whether Sxi2**a** has a similar effect on cell-cell fusion during **a** x **a** unisexual mating
311 (Fig 4A). Interestingly, with the presence of a donor strain (JEC21, *MAT*α, *NAT*^{S} *NEO*^{S}), the fusion
312 frequency between XL280**a** *NAT* and XL280**a** *NEO* was 2.43×10^{-6}, while no significant difference in fusion
313 frequency was found in *sxi2***a**Δ::*NAT* x *sxi2***a**Δ::*NEO* (20% of the wildtype, frequency 5.43×10^{-7}, p-value:
314 0.1204, Welch's t-test). In contrast, the fusion frequencies between *sxi2***a**Δ::*NAT* x XL280**a** *NEO* (7.2-fold
315 higher than wildtype, frequency 1.79×10^{-5}, p-value: 0.0086, Welch's t-test), XL280**a** *NAT* x *sxi2***a**Δ::*NEO*
316 (4.6-fold higher than wildtype, frequency 1.13×10^{-5}, p-value: 0.0002, Welch's t-test) were significantly higher
317 than the wildtype cross (Fig 4C).

318 We hypothesized that NAT and NEO resistant colonies, carrying both selectable markers after cell-
319 cell fusion event, would exhibit diploid DNA content, or triploid if the fusion involved a non-selective donor

320 strain (Fig 4A). To verify the ploidy of fusion products from α x α and **a** x **a** outcrosses, flow cytometry
321 analysis was performed. With *C. neoformans* haploid strain H99 and diploid strain CnLC6683 as controls
322 [50], all NAT- or NEO- containing outcrossing parent strains were confirmed to possess haploid DNA content
323 (Fig 4D). Two independent NAT and NEO resistant colonies from Ménage à trois matings were randomly
324 selected for analysis. As expected in the α x α fusion assay, diploid DNA content was observed in bilateral
325 crosses between *sxi1*αΔ deletion mutants. In contrast, haploid DNA content was detected in XL280α *NAT*
326 x XL280α *NEO* and *sxi1*αΔ::*NAT* x XL280α *NEO* crosses. The presence of haploid NAT and NEO resistant
327 colonies suggests that our assay may slightly overestimate the true frequency of cell-cell fusion events,
328 likely due to genome recombination during unisexual reproduction. Similarly, in **a** x **a** crosses, FACS
329 analysis revealed diploid DNA content in fusion products from XL280**a** *NAT* x XL280**a** *NEO*, *sxi2***a**Δ::*NAT* x
330 *sxi2***a**Δ::*NEO*, and XL280**a** *NAT* x *sxi2***a**Δ::*NEO*, whereas haploid DNA content was found in the *sxi2***a**Δ::*NAT*
331 x XL280**a** *NEO* cross (Fig 4D). To further confirm whether the donor cell directly participated in fusion
332 events, genotyping PCR was performed to amplify *STE20***a** and *STE20*α, allelic variants of the same
333 mating-type-specific genes located with the *MAT* locus. None of the independent fusion products contained
334 the *STE20* allele from the pheromone donor's mating type, indicating that any triploid products involving
335 the donor strain are rare and were not observed in our analysis (Fig 4D and 4E).

336 To dissect the transcriptional differences underlying increased cell fusion frequency, we performed
337 3' enriched RNA-sequencing for wildtype and *sxi1*αΔ bilateral Ménage à trois matings conducted on V8
338 (pH=7) for 72 hours, the identical conditions used for fusion frequency assays. Wildtype samples consisted
339 of XL280α NAT x XL280α NEO x JEC20, while *sxi1*αΔ bilateral samples consisted of *sxi1*αΔ::*NAT* x
340 *sxi1*αΔ::*NEO* x JEC20. Libraries were prepared with a 3' enriched RNA-seq protocol incorporating unique
341 molecular identifiers to enable deduplication and accurate transcript quantification, yielding an average of
342 11.75 million aligned reads per sample (S9 Fig). Principal component analysis revealed clear separation
343 between wildtype and *sxi1*αΔ samples along PC1, which explained 63.2 percent of the variance, while PC2
344 accounted for 19 percent of the variance and showed partial overlap between groups (Fig 4F). Differential
345 expression analysis with an adjusted p-value threshold of 0.05 or less (adjusted p-value<=0.05) and an
346 absolute fold change cutoff of at least two (Fold Change >= 2) identified 134 differentially expressed genes,
347 including 18 upregulated and 116 downregulated genes in *sxi1*αΔ bilateral matings relative to wildtype

348 (Table S1). Consistent with previous findings, the known Sxi1α target *CLP1* was significantly
349 downregulated in *sxi1*αΔ matings. Notably, the pheromone receptor gene *STE3*α and pheromone genes
350 *MF*α*1–3* were significantly upregulated in *sxi1*αΔ matings (Fig 4G). Because genome-wide DEG analysis
351 applies stringent statistical thresholds that may exclude biologically relevant mating and fusion genes, we
352 next examined normalized expression levels using log2 counts per million (CPM) to directly compare
353 transcript abundance across conditions. Examination of log2 CPM for mating and cell fusion related genes
354 confirmed elevated expression of *MF*α*1–3* and *STE3*α, but not for the key transcription factor gene *STE12*α,
355 in *sxi1*αΔ matings. Pheromone genes at the *MAT***a** locus, *MF***a***1–3*, were also upregulated, whereas *STE3***a**
356 and *STE12***a** showed no significant changes (Fig 4H). In addition, significant expression differences were
357 observed for additional Sxi1α targets such as *CPR2* and for key mating regulators *ZNF2* [51] and *CFS1*
358 [52], while no significant differences were detected for *SXI2***a,** *MAT2*, *CVA1* and the fusion associated genes
359 *PRM1* and *KAR5* [53] (Fig 4H).
360

361 **Sxi1α and Sxi2a regulate expression of unique gene subsets in unisexual crosses**

362 To explore potential transcriptional regulatory roles for Sxi1α and Sxi2**a** in unisexual and α x **a**
363 sexual reproduction, we performed RNA-seq of solo-cultures (XL280α, XL280**a**, *sxi1*αΔ, and *sxi2***a**Δ), and
364 co-cultures including a wildtype cross (XL280α x XL280**a**), unilateral crosses (*sxi1*αΔ x XL280**a** and XL280α
365 x *sxi2***a**Δ), and a bilateral mutant cross (*sxi1*αΔ x *sxi2***a**Δ). Reads were mapped to a concatenated assembly
366 consisting of a chromosome-level XL280α genome and the XL280**a** *MAT***a** locus [54], with *MAT***a**- or *MAT*α-
367 masked versions used for solo-cultures and the unmasked assembly for co-cultures. We acquired a mean
368 of 22.4 million reads per sample (SD = 7.6 M) and achieved a mean alignment rate of 95.2% (SD = 0.8%).
369 Genes with at least 1 transcript per million (TPM) in at least one sample were retained for downstream
370 analysis. In both α and **a** solo-cultures, principal component analysis (PCA) of the 500 most variable
371 transcripts showed that the presence/absence of *SXI1*α or *SXI2***a** explained the majority of the variance
372 (S10A and S10B Fig). One replicate from the *sxi1*αΔ solo culture clustered separately from the others in
373 both principal component space and in hierarchical clustering of the relative (scaled variance stabilizing
374 transformation (vst) normalized) expression of the top 500 most variable genes (S10C Fig). Therefore, this
375 replicate was excluded from downstream expression analysis. Re-analysis without this replicate resulted

376 in reduced variance between replicates and a larger proportion of variance explained by PC1 (S10D Fig).
377 All four co-culture crosses showed clear clustering of technical replicates and separation by genotype,
378 indicating that transcriptional differences in these experiments are explained primarily by the independent
379 variable with minimal contributions from confounding variables (S1E Fig). PC1 (62% variance) appears to
380 be explained by the presence of a functional copy of both *SXI1*α and *SXI2***a**, with the samples from the
381 wildtype cross clustering separately from the crosses where one or both genes were deleted. Interestingly,
382 PC2 (25%) shows strong, discrete clustering by genotype, indicating transcriptional differences between
383 crosses lacking *SXI1*α, *SXI2***a**, and both *SXI1*α and *SXI2***a** (S10E Fig).
384 We next performed differential gene expression analysis, treating genes with a false discovery rate
385 (FDR)-adjusted p-value less than or equal to 0.05 and at least a twofold positive or negative expression
386 change as significantly differentially expressed. In the *sxi1*αΔ comparison, *SXI1*α was identified as a DEG,
387 and further analysis of the mapped RNA-seq reads showed that reads mapping to *SXI1*α were concentrated
388 at the same regions with a high mapping rate of the Illumina DNA-seq reads (S11 Fig and Fig 2B). No
389 reads were detected in the open reading frame. This suggests that the 5' UTR region used for homologous
390 recombination may have integrated ectopically in the genome and/or increased in copy number. A *MAT*α-
391 adjacent gene, *FAO1*, was also identified as a DEG in the *sxi1*αΔ solo culture. Reads mapping to this gene
392 were concentrated at the 3' end that was also part of the homology region used for integration of the
393 selectable marker during *SXI1*α gene deletion. It is therefore likely that this effect is also an artifact of
394 ectopic integration of the resistance cassette. Based on these observations, *SXI1*α, *FAO1*, and *SXI2***a** were
395 excluded from consideration as DEGs.
396 In solo-cultures, *sxi1*αΔ had 19 DEGs compared to XL280α, while *sxi2***a**Δ had 23 DEGs relative to
397 XL280**a** (Fig 5A, 5B and Table S2). There were notably no shared DEGs between *sxi1*αΔ and *sxi2***a**Δ (Fig
398 5C). Amt2 (CNJ01880) [55], homologous to a well-characterized ammonium permease required for mating
399 under low-nitrogen conditions in *C. neoformans*, was upregulated in the *sxi1*αΔ mutant. Gene ontology
400 (GO) enrichment analysis of the identified DEGs in the *sxi1*αΔ mutant revealed two significantly enriched
401 terms, *nucleobase transport* and *transmembrane transport* (S12A Fig), whereas no significant enrichment
402 was observed for DEGs from the *sxi2***a**Δ mutant.
403

404 ***SXI1*α and *SXI2*a have distinct and overlapping transcriptional effects in unisexual and** α x **a sexual**
405 **crosses**

406 Given the apparent α- and **a**- specific transcriptional roles of *SXI1*α and *SXI2***a** during unisexual
407 reproduction, we next questioned whether these transcription factors may also function independently of
408 one another, in addition to their known function as a heterodimer, during α x **a** sexual reproduction. We
409 compared transcriptional changes in α x **a** crosses of opposite mating type XL280 parents deficient for one
410 (unilateral cross) or both (bilateral cross) transcription factors. Comparing all mutant crosses to the wildtype
411 cross XL280α x XL280**a**, we identified 336, 190, and 202 DEGs in *sxi1*αΔ x XL280**a**, XL280α x *sxi2***a**Δ, and
412 *sxi1*αΔ x *sxi2***a**Δ, respectively (Table S2). In contrast to the solo-cultures undergoing unisexual reproduction,
413 where the sets of DEGs were markedly smaller and primarily upregulated in *sxi1*αΔ and *sxi2***a**Δ relative to
414 wildtype, DEGs had both increased and decreased expression relative to the XL280α x XL280**a** co-culture
415 cross (Fig 5D-5F). GO term enrichment analysis revealed that DEGs from the unilateral cross *sxi1*αΔ x
416 XL280**a** were predominantly associated with carbohydrate transport and metabolism, including
417 monosaccharide, hexose, and glucose transmembrane transport, as well as carbohydrate catabolic
418 processes (S12B Fig). The unilateral cross XL280α x *sxi2***a**Δ showed enrichment for broader carbohydrate
419 metabolic and catabolic processes (S12B Fig). In the bilateral mutant cross *sxi1*αΔ x *sxi2***a**Δ, enriched
420 terms were similar to those in the *sxi1*αΔ unilateral cross, with strong representation of carbohydrate
421 transport, catabolism, and glucose-related processes (S12B Fig). These results suggest that Sxi1α and
422 Sxi2**a** are involved in broad metabolic regulation during sexual reproduction, evidencing their functionality
423 beyond processes directly implicated in sexual development. Further, observations that deletion of *SXI1*α
424 has a more pronounced impact on carbohydrate-related pathways during mating compared to deletion of
425 *SXI2***a** provide additional support for the existence of distinct roles for these transcription factors.

426 There were eight DEGs in common between solo *sxi1*αΔ cultures and the *sxi1*αΔ x XL280**a** cross
427 and five DEGs in common between solo *sxi2***a**Δ and the XL280α x *sxi2***a**Δ cross (Fig 5G and 5H). These
428 genes are largely uncharacterized, with functions that remain unknown, except for *DHA1* (CND04870) [56],
429 a secreted protein whose expression is regulated by copper availability and which was identified as a DEG
430 in both modes of sexual reproduction in the *sxi2***a**Δ mutant. Comparison of the predicted protein sequences

431 of these shared genes with *S. cerevisiae* proteins shows potential orthologs with roles in metabolic
432 processes (Table S3).

433 Given the enrichment for metabolic processes in the transcriptomic data, we used Biolog YT
434 phenotypic plates to assess whether these changes translated into altered substrate utilization [57,58]. The
435 Biolog YT panel is specifically designed for yeast metabolic phenotyping and contains 94 wells, each
436 preloaded with a different carbon source, enabling comprehensive assessment of both respiratory and
437 growth-based metabolic activity over time. PCA of metabolic activity at 72, 96, and 120 h showed partial
438 separation between *sxi1*αΔ and XL280α (PC1 = 24.4% variance) (S13A Fig), with PERMANOVA confirming
439 a significant difference ($R^2 = 0.123$, $p = 0.026$). *sxi2***a**Δ and XL280**a** showed greater overlap (PC1 = 43%)
440 (S13B Fig), with no significant difference ($R^2 = 0.057$, $p = 0.389$). To pinpoint the substrates contributing to
441 these differences, pairwise t-tests were performed for each carbon source at each time point. In the *sxi1*αΔ
442 mutant, significant differences ($p < 0.05$) compared to XL280α were observed for utilization of D-gluconic
443 acid, D-sorbitol, L-malic acid, N-acetyl-L-glutamic acid plus D-xylose, and palatinose at one or more tested
444 time points (S14 Fig). In the *sxi2***a**Δ mutant, utilization of β-methyl-D-glucoside, gentibiose, quinic acid plus
445 D-xylose, D-galactose, D-raffinose, D-sorbitol, and dextrin differed significantly from XL280**a** in at least one
446 of the tested time points (S15 Fig). These phenotypic differences in carbon source utilization are consistent
447 with the RNA-seq GO term enrichment results, which indicated that the Sxi1α and Sxi2**a** mutations affect
448 genes involved in carbohydrate transport and metabolism.

449 The identification of shared DEGs between unisexual and α x **a** sexual crosses indicates that Sxi1α,
450 and potentially Sxi2**a**, could have distinct transcriptional effects from their heterodimer interacting partner.
451 These observations, coupled with the computational prediction and yeast two-hybrid assays that Sxi2**a** may
452 be capable of forming homodimers, led us to question the extent of Sxi1α- and Sxi2**a**-dependent
453 transcriptional effects occurring independently of the presence of a functional heterodimer interacting
454 partner during α x **a** crosses. To differentiate between transcriptional events dependent on the Sxi1α-Sxi2**a**
455 heterodimer as opposed to only Sxi1α or only Sxi2**a**, we examined the direction of differential expression
456 in DEGs identified in one or more crosses (Fig 6A). Compared to the XL280α x XL280**a** cross, candidate
457 heterodimer-regulated genes should undergo either a positive (heterodimer-repressed) or negative
458 (heterodimer-activated) change in expression in crosses lacking *SXI1*α, *SXI2***a**, or both (Fig 6A, top panel).

459 By these criteria, we identified 57 and 65 potential heterodimer-repressed and -activated genes,
460 respectively (Fig 6A, top panel). Consistent with previous reports [26,29], *CLP1* (CNB01190) was among
461 the set of heterodimer-activated genes. We next reasoned that any genes whose expression depends only
462 on Sxi1α would have either increased (Sxi1α-repressed) or decreased (Sxi1α-activated) expression relative
463 to wildtype in the *sxi1*αΔ x XL280**a** cross, but no expression change in the XL280α x *sxi2***a**Δ cross because
464 XL280α has a functional copy of Sxi1α (Fig 6A, middle panel). Strikingly, we identified a larger gene set
465 that fit these criteria than potential heterodimer-regulated genes, with 78 and 109 Sxi1α-activated and -
466 repressed DEGs, respectively (Fig 6A, middle panel). Lastly, we applied similar reasoning to identify DEGs
467 whose expression depends only on a functional copy of *SXI2***a** (Fig 6A, bottom panel). From this
468 comparison, we identified 14 and 27 potential Sxi2**a**-activated and -repressed genes, respectively (Fig 6A,
469 bottom panel). Surprisingly, *CPR2* (CNB04250) [27], a gene thought to be activated by the Sxi1α-Sxi2**a**
470 heterodimer, was present in the set of 27 genes with potential Sxi2**a**-dependent activation.
471
472 ***SXI1*α and *SXI2*a have distinct regulatory effects on the α and a *MAT* loci**
473 We observed an enrichment of *MAT*α and *MAT***a** genes in the Sxi1α- and Sxi2**a**-only dependent
474 sets of DEGs compared to the heterodimer set, in which only two genes (*MF***a***1* and *MF***a***2*) were predicted
475 to be heterodimer repressed (Fig 6A, top panel). Plotting expression change in all crosses for the *MAT*α
476 and *MAT***a** loci revealed an even more surprising pattern, where a majority of genes in each locus appear
477 to be controlled by Sxi1α and Sxi2**a** in opposing directions. *MAT*α genes tend to have increased expression
478 in the absence of Sxi1α and decreased expression in the absence of Sxi2**a**, suggesting a negative
479 regulatory role for Sxi1α and a positive regulatory role for Sxi2**a** (Fig. 6B). Conversely, *MAT***a** genes
480 generally have positive expression changes in the absence of Sxi2**a** and negative expression changes in
481 the absence of Sxi1α (Fig. 6C). In the case of *MAT***a** genes, expression differences in the *sxi1*αΔ x *sxi2***a**Δ
482 crosses more closely mirror those in the XL280α x *sxi2***a**Δ than in *sxi1*αΔ x XL280**a**. Therefore, while *sxi2***a**Δ
483 may result in a smaller set of uniquely differentially expressed genes, Sxi2**a** may have an important role in
484 driving *MAT***a** gene expression change in opposition to Sxi1α. Taken together, these results support distinct
485 roles for *SXI1*α and *SXI2***a** in both mating-type-specific and more general gene regulation.

Discussion

The AlphaFold3-predicted heterodimer structure of Sxi1α and Sxi2**a** closely resembles the yeast **a**1-α2 complex [40] and the predicted *U. maydis* bW-bE heterodimer, consistent with prior studies [2,22]. This apparent conservation across diverse yeast species supports an evolutionarily important role of the Sxi1α-Sxi2**a** complex in α x **a** mating. Lower-confidence predictions indicate that Sxi1α and Sxi2**a** may also form homodimers, similar to α2 in *S. cerevisiae*, raising the possibility of independent, non-heterodimer functions. Importantly, results from yeast two-hybrid assay support functional asymmetry between the two HD proteins. Whereas HD2 Sxi2**a** appears capable of forming a homodimer, comparable homodimerization by HD1 Sxi1α has not been observed. This distinction suggests that Sxi2**a** may possess a greater capacity for autonomous regulatory activity, while Sxi1α may depend more strongly on alternative co-factors or context-specific interactions. Such asymmetry provides a potential mechanistic explanation for the opposing and gene-specific regulatory effects of Sxi1α and Sxi2**a** observed across multiple mating contexts. Interestingly, homodimerization of HD2 has been reported in the homothallic fungus *Cystofilobasidium capitatum*, where HD2 homodimers can substitute for the canonical HD1-HD2 heterodimer and thereby provide an alternative mechanism for regulating sexual reproduction [59]. Likewise, in the basidiomycetous yeast *Phaffia rhodozyma*, the homeodomain proteins HD1 and HD2 display only a weak heterodimer interaction, while experimental assays revealed potential homodimer formation [60]. In contrast, in *Ustilago maydis* the bE and bW homeodomain transcription factors strictly function through non-self heterodimerization, and no evidence for functional homodimerization has been found [61]. These examples suggest that HD homodimerization, although rare, may provide lineage-specific solutions for regulating sexual development. Together with our transcriptomic findings, this led us to hypothesize that these transcription factors can act both together and separately, whether as homodimers or by another means regulating mating before and after cell-cell fusion in unisexual and α x **a** reproduction.

Our transcriptomic results provide further evidence for this model, as we observed Sxi2**a**-independent transcriptional regulation by Sxi1α and Sxi1α-independent regulation by Sxi2**a** in both unisexual and α x **a** sexual matings. In addition to regulating largely distinct gene sets, Sxi1α and Sxi2**a** exert contrasting effects on the two mating-type loci. We observed an enrichment of *MAT*α and *MAT***a** genes in the Sxi1α-only and Sxi2**a**-only dependent DEG sets in α x **a** crosses, whereas the heterodimer-

514 dependent set contained only two repressed genes (*MF***a***1* and *MF***a***2*). Strikingly, most *MAT*α genes
515 showed increased expression in the absence of *Sxi1*α but decreased expression in the absence of *Sxi2***a**,
516 suggesting that Sxi1α functions primarily as a negative regulator and Sxi2**a** as a positive regulator at this
517 locus. The pattern was reversed for *MAT***a** genes, with *Sxi1*α acting positively and *Sxi2***a** negatively. These
518 results indicate that, beyond their shared role as a heterodimer, Sxi1α and Sxi2**a** also engage in mating-
519 type-specific regulatory programs that act in opposition to each other, potentially fine-tuning the expression
520 of *MAT*-linked genes during α x **a** sexual reproduction. Deletion of Sxi1α caused an increase in α-α cell
521 fusion, consistent with a functional role beyond that of Sxi1α-Sxi2**a** heterodimer. To further interpret the
522 molecular basis of altered fusion frequency, we considered transcriptional changes associated specifically
523 with fusion-competent mating conditions. Under these conditions, genes involved in pheromone sensing
524 and signaling, including the pheromone receptor gene *STE3* and multiple pheromone genes, were
525 upregulated, whereas canonical membrane fusion and karyogamy genes such as *PRM1* and *KAR5* [53]
526 did not show corresponding induction. This pattern suggests that enhanced fusion may arise from elevated
527 mating competence or increased responsiveness to pheromone cues rather than from direct transcriptional
528 activation of the fusion machinery itself. Such regulation at the level of upstream signaling could provide a
529 flexible mechanism for modulating fusion probability without broadly altering the core fusion apparatus.
530 These results support the possibility that Sxi1α may act independently of Sxi2**a**, and future work will
531 continue to explore potential co-factors/interacting partner(s). In α x **a** reproduction, both Sxi1α and Sxi2**a**
532 are essential for normal hyphal development and sporulation in multiple genetic backgrounds [2,22]. In
533 contrast, in the XL280 background, deletion of either gene did not impair unisexual colony morphology or
534 sporulation. These results, coupled with the observation of *SXI1*α - and *SXI2***a**-dependent transcriptional
535 activity during unisexual and α x **a** sexual reproduction, suggest that these transcription factors are active
536 but may play distinct roles in α x α and **a** x **a** versus α x **a** reproduction, and that unisexual reproduction is
537 likely regulated in a manner that is at least partially distinct from α x **a** sexual reproduction. This is also
538 consistent with recent reports that Sxi2**a** is dispensable for unisexual reproduction in *C. neoformans* [31].
539 Functional differences between the two HD proteins were most evident in unisexual fusion assays.
540 Sxi1α inhibited fusion in both unilateral and bilateral mutant crosses, whereas Sxi2**a** inhibition was observed
541 only in unilateral crosses. This may indicate that Sxi2**a** plays a less-prominent or context-dependent role

542 in **a** x **a** cell fusion, possibly masked in bilateral crosses by redundancy with other transcription factors.
543 Testing this possibility will require identifying Sxi2**a**'s non-Sxi1α partners and determining their contributions
544 to fusion regulation.

545 Our transcriptomic analysis identified distinct subsets of Sxi1α- and Sxi2**a**-regulated genes in both
546 unilateral and bilateral crosses. A majority of these genes remain uncharacterized, inviting future functional
547 investigation into their potential involvement in cell-cell fusion and sexual reproduction. Notably, GO term
548 enrichment highlighted metabolism-related processes, and Biolog YT plate profiling revealed subtle but
549 reproducible shifts in carbon source utilization between wildtype and mutants. Together, these findings
550 suggest that Sxi1α and Sxi2**a** influence metabolic pathways, which may, in turn, modulate mating efficiency
551 under nutrient-variable conditions, thereby linking metabolic state to the mating regulatory network and
552 highlighting carbohydrate metabolism as an important area for future investigation of Sxi1α and Sxi2**a**
553 function.

554 By analyzing 341 *MAT*α clinical and environmental isolates out of the total 387 isolates in the *C.*
555 *neoformans* Strain Diversity Collection [33] through a similar pipeline [62] as reported in our previous work
556 [63], we found there were only two closely related environmental isolates (Muc504-1 and Muc489-1) that
557 harbored an identical high-impact nonsense mutation in the *SXI1*α gene, resulting in truncation of the C-
558 terminal 23 amino acids. The widespread conservation of this gene suggests that it is under positive
559 selection and likely has important functions in a variety of ecological contexts. Unisexual reproduction,
560 which allows cells to produce stress-resistant spores under harsh environmental conditions in the absence
561 of an opposite mating type partner, provides one hypothetical avenue by which sex-specific genes like
562 *SXI1*α could continue to be selected for in a predominantly *MAT*α population. While the inhibitory role of
563 Sxi1α on unisexual α-α fusion could, in principle, be expected to limit the expansion of *MAT*α lineages and
564 favor *MAT***a** cells, this prediction appears inconsistent with the observed predominance of *MAT*α in natural
565 populations. This paradox suggests that additional mechanisms beyond Sxi1α regulation must contribute
566 to shaping the observed mating-type distribution. Further studies are needed to clarify the downstream
567 regulators involved in the novel repressive role of Sxi1α in unisexual reproduction and other potential
568 mating-independent functions. These lines of investigation have the potential to elucidate fitness-
569 enhancing strategies employed by this organism to undergo unisexual meiosis and produce infectious

570 spores. Over evolutionary time, it is conceivable that selection for alternative reproductive strategies such
571 as unisexual reproduction could have contributed to the widespread dominance of *MAT*α strains. In this
572 context, we speculate that repression of α–α cell fusion by the α-specific homeodomain protein Sxi1α
573 represents a *Cryptococcus*-specific evolutionary adaptation that fine-tunes unisexual development to permit
574 efficient spore production in the absence of a conidiospore-based asexual program. Such a mechanism
575 may balance the selective advantage of abundant basidiospore formation with controlled mating behavior
576 under partner-limited conditions.

577 In *S. cerevisiae*, the α2 transcription factor functions both as a homodimer and heterodimer with
578 **a**1, playing key roles in mating-type regulation [6–9]. The transcriptional regulation of **a**-specific and
579 haploid-specific genes involves interactions with the transcription factor Mcm1 [6,43]. Given this precedent,
580 a similar dual functionality with/without mating partner may exist for the sex-specific HD transcription factor
581 Sxi1α in *Cryptococcus*, and non-Sxi2**a** interacting partners may exist. Interestingly, orthologs of *S.*
582 *cerevisiae* Mcm1 are also present in *C. neoformans* and *C. deneoformans*, where they have been reported
583 to function in α x **a** sexual reproduction [49]. However, our functional analysis suggests that the
584 *Cryptococcus* Mcm1 ortholog does not play a central role in *Cryptococcus* mating under the conditions
585 examined. In contrast to its well-established function in budding yeast, loss of Mcm1 did not result in clear
586 defects in unisexual or α x **a** sexual reproduction. Together with the absence of strong evidence for direct
587 association with either Sxi1α or Sxi2**a**, these observations indicate that *Cryptococcus* mating circuits have
588 diverged substantially from the canonical budding yeast α2–Mcm1 regulatory framework, relying instead
589 on alternative or redundant transcriptional circuits. Our results suggest that Sxi1α might act as both a
590 positive (e.g., in α x **a** mating development) and a negative regulator (e.g., in α x α cell fusion and over
591 transcription of certain *MAT* genes) [23]. This phenomenon is reminiscent of the mitogen-activated protein
592 kinase Kss1 in *S. cerevisiae*, which regulates pseudohyphal differentiation through complex signaling
593 mechanisms and functions as a multifunctional regulator in fungal development with counter-balanced
594 positive and negative roles [64]. Efforts to identify potential Sxi1α - and Sxi2**a** - specific transcription factor
595 binding sites in the promoter regions of differentially expressed genes were not successful, likely due to the
596 presence of numerous derivative consensus sequences (similar to what has previously been observed in
597 *C. neoformans*), as well as the potential activation of regulatory cascades as a result of changes in Sxi1α

598 and Sxi2**a** activity, meaning that many promoters of DEGs are not bound by the homeodomain proteins
599 themselves. Future efforts to elucidate direct targets of the heterodimer and putative homodimers will
600 involve ChIP-seq–based experimental validation of binding sites in the presence and absence of each
601 transcription factor, ideally integrated with transcriptomic analyses to distinguish direct from indirect
602 regulatory effects.

603 While the HD proteins Sxi1α and Sxi2**a** are dispensable for colony morphology, sporulation, and
604 cell viability during unisexual reproduction, Sxi1α plays a key inhibitory role in α x α cell fusion, and the
605 contribution of Sxi2**a** to this process appears to be more limited. RNA-seq analysis further revealed that
606 the heterodimer partners also have distinct and independent regulatory programs, supporting functional
607 roles beyond their shared activity as a complex. These findings suggest that Sxi1α may have novel
608 functions during *Cryptococcus* mating that are yet to be characterized, potentially analogous to those in
609 other well studied fungal species, and highlight an additional facet in the complex regulation of sexual
610 reproduction in this important human fungal pathogen. Our findings also raise important questions
611 regarding the functional conservation of sex-specific homeodomain proteins in ascomycetes and
612 basidiomycetes. Future studies will investigate protein complexes involving Sxi1α, Sxi2**a**, and additional
613 interacting partners to elucidate the extent of conservation with well-characterized homeodomain
614 complexes such as **a**1-α2 in *S. cerevisiae*. Collectively, these findings support a model in which Sxi1α and
615 Sxi2**a** act through partially independent regulatory programs that modulate pheromone signaling,
616 transcriptional responsiveness, and developmental timing, rather than functioning exclusively as an obligate
617 heterodimeric switch. Taken together, our findings demonstrate that gene regulation by Sxi1α and Sxi2**a** is
618 more complex than previously appreciated and provide a foundation for future molecular analyses aimed
619 at further delineating the *Cryptococcus* developmental program.

620 **Materials and methods**

621 **Fungal strains and growth conditions**

622 *C. deneoformans* and *C. neoformans* strains for this study are listed in Table S4. The strains were
623 stored in 15% glycerol at -80°C for long-term storage. Fresh strains were streaked from glycerol stocks
624 and maintained on solid YPD medium (1% yeast extract, 2% Bacto Peptone, 2% dextrose) at 30°C.

625 Spot dilution assays were performed with overnight cultures of the tested strains grown in liquid
626 YPD at 30°C. Strains were diluted to an OD_{600} of 0.5 in sterile water. These cultures were further serially
627 diluted 5-fold and spotted (3 µL for each dilution) onto YPD plates. The plates were incubated at 30°C and
628 37°C (testing thermotolerance) for 2 days before imaging.

629

630 **Protein structural predictions**

631 Protein structure predictions were made with AlphaFold3 [65] on the AlphaFold server
632 (https://alphafoldserver.com/). The predicted models and error plots were further processed with Chimera
633 X (v 1.9) [66] for predicted local distance difference test (pLDDT) value filtering, alignment, and visualization.

634

635 **Yeast two-hybrid assay**

636 Sxi1α, Sxi2**a**, and Sxi2**a**N constructs were generated previously [2]. Briefly, *SXI1*α and *SXI2***a**
637 coding sequences from XL280 were cloned from cDNA into Gal4 DNA-binding domain (GBD) and Gal4
638 activation domain (GAD) vectors, and truncated *SXI2***a** fragments were generated by PCR amplification of
639 the defined N-terminal region (encoding amino acids 1-217). For this study, the putative *C. deneoformans*
640 *MCM1* coding sequence was amplified from XL280 cDNA and cloned into GBD and GAD vectors to
641 generate yeast two-hybrid constructs. All previously generated and newly constructed plasmids were
642 sequence-verified prior to use (Table S4). Reporter strains Y2HGold and Y187 were transformed with
643 plasmids via the high-efficiency transformation method [67]. Diploids were generated by mating and
644 selected for on synthetic dextrose (SD) dropout medium (0.67% yeast nitrogen base, 2% dextrose) minus
645 leucine and tryptophan. Adenine sulfate was added to the medium at a concentration of 20 mg/L, and
646 amino acids and uracil were included at standard concentrations to support auxotrophic growth
647 requirements. Gal4-dependent activation of *ADE2* and *HIS3* reporter genes was assessed by growth on

648 SD medium additionally lacking adenine or histidine, respectively. β-galactosidase activity was measured
649 using a chlorophenol red-β-D-galactopyranoside (CPRG)–based liquid assay (OZ Biosciences) according
650 to the manufacturer's instructions. Absorbance was measured at 595 nm, and enzyme activity (milliunits)
651 was calculated based on a linear standard curve.
652
653 **Gene deletion and confirmation**
654 Approximately 1.0 kb 5' and 3' flanking regions of the *SXI1*α gene and 60 bp 5' and 3' flanking
655 regions of the *SXI2***a** and *MCM1* gene were constructed with primers listed in Table S5 to target their
656 respective genes in XL280 for homologous recombination [46]. Overlap PCR with a selectable marker was
657 used to construct the DNA donor with 1.0 kb homology, while 60 bp microhomology was included in the
658 primers for donor amplification. *C. neoformans* codon optimized Cas9, gRNAs (a single gRNA targeting
659 *SXI1*α and two gRNAs targeting *SXI2***a**), and drug resistance cassettes (*NAT* from pAI3 or *NEO* from pJAF1)
660 containing homologous flanking sequences were introduced into XL280 wildtype strains via the previously
661 reported Transient CRISPR-Cas9 Coupled with Electroporation (TRACE) system [38,39]. Transformants
662 were screened with PCR internal to the ORF, and 5′ and 3′ junction PCR to the drug resistance marker
663 integration sites to confirm integration at the genomic locus. Illumina whole-genome sequencing was
664 performed on positive transformants with Novaseq X Plus platform (2x150 bp). The sequencing reads were
665 mapped to a modified version of the XL280α genome [54] with the Burrows-Wheeler Alignment tool (BWA)
666 (v 0.7.17) [68] to further confirm the deletion mutant strains. The modification included adding the *MAT***a**
667 locus sequence of JEC20 (GenBank: AF542530.2) as an additional contig.
668 H99 *mcm1*Δ was obtained from [49] and crossed with KN99**a** to obtain KN99**a** *Mcm1*Δ. Both
669 mutants were verified by internal PCR targeting the *MCM1* ORF with the primers listed in Table S5.
670
671 **Capsule formation and melanin production assays**
672 Tested strains, with an initial OD_{600} of 0.1 in 4 mL liquid RPMI medium (RPMI 1640 with 2%
673 dextrose), were incubated on a roller drum at 70 rpm and 30°C for 3 days. After washing and resuspension
674 in water, the cells were negatively stained with an equal volume of India ink to visualize the capsules.

675 To assess melanin production, overnight saturated cultures of test strains were spotted (10 μL)
676 onto Niger seed agar plates (7% Niger seed, 0.1% dextrose). The Niger seed plates were incubated at
677 30°C and 37°C for 8 days before photographing.
678
679 **Competition assays**
680 Overnight cultures of tested strains grown in liquid YPD at 30°C were diluted to OD_{600} of 0.2 and
681 equally mixed in a 1:1 ratio in 5 mL of liquid YPD for co-culture. *sxi1*αΔ::*NAT* mutants (resistant to NAT)
682 and *sxi2***a**Δ::*NEO* mutants (resistant to NEO) were mixed with XL280α and XL280**a**, respectively. The
683 mixture was plated on YPD plates, YPD + nourseothricin (NAT), and YPD + neomycin (NEO) to confirm
684 starting ratio. After 24 and 48 hours of co-culture, an aliquot of the mixture was sampled, and plating was
685 repeated with OD_{600} diluted to 0.1 to track changes in relative abundance of mutants. Four independent
686 replicates were performed for each competition.
687 For the competition assay performed on MS medium, overnight cultures were similarly diluted to
688 OD_{600} of 1. *sxi1*αΔ::*NAT* or *sxi2***a**Δ::*NEO* mutants and the corresponding XL280 wildtype strain were equally
689 mixed in a 1:1 ratio and spotted on MS medium. Spores were dissected 10 to 14 days post spotting. Yeast
690 cells from internal regions were also collected. Spores or yeast cells were further transferred to YPD+NAT,
691 YPD+NEO and YPD to determine the ratio of mutants in the population. Five independent spots were
692 investigated for each competition.
693
694 **Mating and cell-cell fusion assay**
695 Mating plates were set up as described previously [69]. α x α and **a** x **a** unisexual reproduction
696 assays were performed on Murashige and Skoog (MS, Sigma, USA) plates for 1 to 2 weeks before imaging
697 and dissection. Basidiospores generated during unisexual reproduction were randomly dissected and
698 plated on YPD plates for 2 to 3 days to determine spore viability and germination rates.
699 Cell-cell fusion frequency during α x α unisexual outcrossing in XL280α *NAT* (XL561 and XL562)
700 and XL280α *NEO* (XL563 and XL564) was compared to bilateral mutant crosses of *sxi1*αΔ::*NAT* and *sxi1*αΔ:
701 *NEO* or unilateral crosses of *sxi1*αΔ::*NAT* and XL280α *NEO*. Similarly, **a** x **a** unisexual outcrossing in
702 XL280**a** *NAT* (CF1816) and XL280**a** *NEO* (JHG223) was compared to bilateral mutant crosses of

703 *sxi2***a**Δ::*NAT* and *sxi2***a**Δ::*NEO* or unilateral crosses of *sxi2***a**Δ::*NAT* and XL280**a** *NEO* or *sxi2***a**Δ::*NEO* and
704 XL280**a** *NAT*.
705 Cells were diluted in sterile water to an OD_{600} of 1. Two *MAT*α strains (α x α outcrossing) or *MAT***a**
706 strains (**a** x **a** outcrossing) containing either *NAT* or *NEO* resistance cassettes were mixed equally with
707 JEC20 (*MAT***a**) or JEC21 (*MAT*α) for Ménage à trois matings on V8 agar (pH=7) and incubated for 72 hours
708 in the dark at room temperature. The cells were then collected and plated on YPD + NAT (100 µg/mL) +
709 NEO (200 µg/mL) and YPD alone to determine the ratio of colonies with dual resistance four to five days
710 post-plating (i.e., fusion product) out of the total cells. Genotypes at mating type locus of the fusion products
711 was validated via *STE20***a** or *STE20*α genotyping PCR.
712
713 **Flow cytometry analysis**
714 Ploidy of the fusion products from α x α or **a** x **a** cell fusion was determined by fluorescence-
715 activated cell sorting (FACS) analysis as previously described [70]. Cells were grown overnight on solid
716 YPD medium at 30 °C, harvested, and washed with 1 mL PBS. The cells were fixed in 70% ethanol at 4 °C
717 overnight, pelleted and washed with 1 x NS buffer (10 mM Tris-HCl pH=7.5, 0.25 M sucrose, 1 mM EDTA,
718 1 mM $MgCl_2$, 0.13 mM $CaCl_2$, 0.1 mM $ZnCl_2$, 0.5 mM phenylmethylsulfonyl fluoride, 7 mM β-
719 mercaptoethanol). Samples were treated with RNase A (1.05 mg/mL) and stained with propidium iodide
720 (PI, 30 µg/mL) in a total volume of 200 µL 1x NS solution. Stained cells were diluted in 1x Tris-PI buffer
721 (0.964 M Tris-HCl pH=7.5, 35 µg/mL PI) prior to analysis. FACS was performed at Duke Cancer Institute
722 Flow Cytometry Core Facility with approximately 10,000 cells analyzed per sample. Flow cytometry data
723 were visualized using FlowJo (v.10.10.0).
724
725 **Light and scanning electron microscopy (SEM)**
726 Mating structures from MS plates were imaged with an AxioSkop 2 fluorescence microscope to
727 visualize hyphae, basidia and basidiospores under brightfield. SEM samples were prepared following a
728 previously described protocol [50] with minor modifications. Briefly, a ~2 cm x 2 cm agar plug containing
729 patch of mated cells from MS plates was fixed in PBS containing 4% formaldehyde and 2% glutaraldehyde
730 at 4°C for 2 hours. The fixed samples were then gradually dehydrated in a graded ethanol series (30%,

731 50%, 70%, 95%), with each step performed at 4°C for 15 min. This was followed by three washes in 100%
732 ethanol, each at 4°C for 15 min. The samples were further dehydrated with a Ladd CPD3 Critical Point
733 Dryer and subsequently coated with a thin layer of gold with a Denton Desk V Sputter Coater (Denton
734 Vacuum, USA). Hyphae, basidia and basidiospores were observed with a scanning electron microscope
735 equipped with an EDS detector (Apreo S, ThermoFisher, USA).
736
737 **RNA preparation and sequencing**
738 For Ménage à trois matings, cells were diluted in sterile water to an OD_{600} of 1. Two *MAT*α strains
739 (α x α outcrossing) containing either *NAT* or *NEO* resistance cassettes were mixed equally with JEC20
740 (*MAT***a**) on V8 agar (pH = 7) and incubated for 72 hours in the dark at room temperature after harvesting.
741 Three biological replicates were performed for each strain or mating pair. Harvested samples were
742 lyophilized and processed for RNA extraction using the RNeasy Mini Kit (Qiagen), following the
743 manufacturer's instructions. Library preparation and sequencing was performed by Plasmidsaurus (USA).
744 RNA libraries were generated from total RNA using a strand-specific 3' end counting protocol with unique
745 molecular identifiers (UMIs) to enable accurate transcript abundance quantification
746 (https://plasmidsaurus.com/rna). Libraries were sequenced on the Illumina platform, yielding deduplicated
747 3' end enriched reads for gene expression analysis.
748 For both unisexual and α x **a** sexual crosses, strains were collected from 2 to 3-day-old cultures
749 grown on solid YPD medium and diluted to an OD_{600} of 1. For unisexual crosses, 10 µL of the diluted culture
750 ($OD_{600=}$1) was spotted onto V8 agar plates (pH= 7), with 10 spots per plate and three technical replicate
751 plates per biological replicate. For α x **a** crosses, equal volumes of *MAT*α and *MAT***a** cell suspensions
752 (each at $OD_{600=}$1) were mixed prior to spotting under the same conditions. Three biological replicates were
753 performed for each strain or mating pair. Plates were incubated at room temperature for 72 hours in the
754 dark, after which cells were washed off and collected. Harvested samples were lyophilized and processed
755 for RNA extraction using the RNeasy Mini Kit (Qiagen), following the manufacturer's instructions.
756 RNA was sequenced by the Duke University Sequencing and Genomic Technologies Core Facility.
757 Poly-A enriched libraries were prepared from samples with RIN ≥ 7 using the Kapa mRNA-seq HyperPrep

758 kit (Kapa Bioscience). Pooled libraries were sequenced on an Illumina Novaseq X Plus instrument in 150
759 bp paired-end reads.
760
761 **RNA-sequencing data analysis**
762 For Plasmidsaurus RNA-seq, data was analyzed following Plasmidsaurus's instructions. Briefly,
763 raw reads were quality filtered by fastp (v0.24.0) [71], then aligned to the XL280α reference genome with
764 an additional *MAT***a** sequences from JEC20 using STAR aligner (v.2.7.11b) [72], with non-canonical splice
765 junction disallowed. PCR duplication was removed through UMI-based deduplication with UMIcollapse
766 (v1.1.0) [73]. Alignment quality metrics, strand specificity, and read distribution across genomic features
767 including enrichment toward transcript 3' ends were assessed using RSeQC (v5.0.4) [74] and Qualimap
768 (v2.3) [75], with results aggregated into a comprehensive quality control report using MultiQC (v1.32) [76].
769 Gene-level expression quantification was performed by using featureCounts (v2.1.1) [77]. PCA were
770 calculated on normalized counts (TMM, trimmed mean of M-values) using Pearson correlation. Differential
771 expression was done with edgeR [78] (v4.0.16) using standard practice including filtering for low-expressed
772 genes with edgeR::filterByExprwith default values. Differentially expressed genes (DEGs) were identified
773 using a significance threshold of adjusted p-value <= 0.05 and an absolute $\log_2$ fold change cutoff of 1.
774 FeatureCounts gene level counts were filtered and TMM normalized using edgeR, and $\log_2$ counts per
775 million (CPM) values were calculated. Significance was determined using Welch two sample t-tests with
776 Benjamini Hochberg false discovery rate correction.
777 For RNA-seq data from both unisexual and α x **a** sexual crosses, Illumina universal adaptors were
778 trimmed from paired reads with CutAdapt (v4.9) [79]. Trimmed reads were aligned to the XL280α + *MAT***a**
779 concatenated reference assembly. Modified assemblies with *MAT*α (Chr4 coordinates 1522691-1656182)
780 and *MAT***a** (MATa coordinates 0-148067) masked were generated by using the bedtools (v2.31.1)
781 maskfasta function on the concatenated assembly [80]. XL280α background unisexual crosses were
782 mapped to the *MAT***a**-masked assembly, XL280**a** background unisexual crosses to the *MAT*α-masked
783 assembly, and α-**a** sexual crosses to the full, unmasked assembly with HISAT2 (v2.2.1) [81]. Counts per
784 gene were quantified with featureCounts (v2.0.6) [77] with a gff annotation file generated by Liftoff (v1.6.3)
785 [82] of annotated features from JEC20 and JEC21 [83].

786 Exploratory data analysis and differential expression analysis were performed with DESeq2
787 (v1.44.0) [84]. Prior to analysis, transcript counts were normalized by transcripts per million (TPM) within
788 each replicate and genes with at least 1 TPM in 1 sample were retained. Clustering and principal
789 component analyses were performed using vst normalized values for the top 500 most variable genes
790 generated by DESeq2. Differential expression analysis was carried out in DESeq2 with alpha = 0.05 and
791 a $\log_2$FC cutoff of +/- 1 was applied to identify DEGs from the resulting expression data. The R packages
792 EnhancedVolcano (v1.22.0) (https://github.com/kevinblighe/EnhancedVolcano) and pheatmap (v1.0.13)
793 (https://github.com/raivokolde/pheatmap) were used for data visualization. DEG sets were analyzed with
794 the FungiDB (https://fungidb.org/fungidb/app) GO Enrichment tool using the JEC21 genome as background.
795 Significance was assessed using Fisher's exact test with Benjamini-Hochberg correction, retaining terms
796 with FDR < 0.05. Enriched terms were visualized in RStudio as dot plots ranked by $\log_2$(fold enrichment)
797 or FDR, colored by $-\log_{10}$(FDR), and annotated with gene counts.
798
799 **Biolog phenotypic assays**
800 Overnight cultures grown on solid YM agar (5 g peptone, 3 g yeast extract, 3 g malt extract, 10 g
801 dextrose, 20g agar, pH=6.2) were collected and diluted in sterile water to an OD_{600} of 0.2. A volume of 100
802 µL of the diluted samples was inoculated into each well of the Biolog Yeast Identification Test Panel (YT
803 Microplate) and cultured at 28 °C in the dark. Three biological replicates were performed for each strain.
804 Cell growth was monitored daily with SpectraMax iD3 plate reader at OD_{590} (oxidation test) and
805 OD_{600} (Assimilation test). Growth on each substrate was normalized using the formula (Abs_sample -
806 Abs_water)/(Abs_glucose-Abs_water). Principal component analysis (PCA) was performed using scaled
807 data from Biolog YT plate assays. Differences in global metabolic profiles between genotypes were
808 assessed using PERMANOVA (adonis2 function, vegan R package), with 999 permutations and Euclidean
809 distance as the dissimilarity metric.
810
811
812
813

814 **Statistical analysis**

815 Spore germination and unisexual competitiveness were analyzed with paired or unpaired student
816 t-tests in Rstudio (version 2024.04.1) with the “t.test” function with argument “paired = TRUE” for paired
817 tests or “paired = FALSE” for unpaired tests.

818 Fusion efficiency data were analyzed in RStudio (version 2024.04.1). Welch’s t-tests were
819 performed using the t.test function with the argument “var.equal = FALSE” to compare fusion rates between
820 selected sample groups. Mean values and standard deviations were plotted using ggplot2, with individual
821 data points overlaid.

822 **Data availability**

823 Raw WGS sequencing and RNA-seq reads have been deposited in Bioproject: PRJNA1219566.
824 Scripts associated with RNA-seq data from both unisexual and α x **a** sexual crosses are available at:
825 https://github.com/annalehmann/XL280_Sxi_transcriptome. Scripts related to Plasmidsaurus RNA-seq
826 analysis are available at: https://github.com/Jhuang90/Huang-et-al.-Sxi1_Plasmidsaurus-RNA-seq-script.

827

828 **Acknowledgments**

829 We thank Anna Floyd Averette for constant support, Connor Larmore for critical reading, Dr. Marco
830 Dias Coelho for constructive criticism on the manuscript and suggestions on data presentation, Moayad
831 Shehadeh and Dr. Zhuyun Bian for technical support, and all of the members of the Heitman Lab for
832 constructive suggestions. We also thank Dr. Xiaorong Lin (University of Georgia) for sharing the XL280
833 congenic strains, Dr. Ruiyun Zeng (North Carolina State University) for assistance in data visualization, Dr.
834 Paul Magwene and Claudia Zirión Martinez (Department of Biology, Duke) for sharing unpublished pipeline
835 for variant detection from Strain Diversity Collection, Dr. Bin Li (Duke Cancer Institute Flow Cytometry Core
836 Facility), Julian Liber (Department of Biology, Duke), and Dr. Devi Swain Lenz (Duke's Sequencing and
837 Genomic Technologies Core Facility) for advice and expertise.

838

839 **Funding**

840 This study was supported by NIH/NIAID R01 grants (AI039115-28, AI050113-20, and AI133654-07.
841 to J. Heitman) J. Heitman is co-director and fellow of the Canadian Institute for Advanced Research (CIFAR)
842 program Fungal Kingdom: Threats & Opportunities. The funders had no role in study design, data collection
843 and analysis, decision to publish, or preparation of the manuscript.

844

845 **Competing interests**

846 I have read the journal's policy and the authors of this manuscript have the following competing
847 interests:. All other authors have declared that no competing interests exist.

848 **References**

849 1. Coelho MA, David-Palma M, Marincowitz S, Aylward J, Pham NQ, Yurkov AM, et al.
850 Tracing the evolution and genomic dynamics of mating-type loci in *Cryptococcus*
851 pathogens and closely related species. bioRxiv; 2025.
852 doi:10.1101/2025.02.12.637874

853 2. Hull CM, Boily M-J, Heitman J. Sex-Specific homeodomain proteins Sxi1α and Sxi2**a**
854 coordinately regulate sexual development in *Cryptococcus neoformans*. Eukaryot
855 Cell. 2005;4: 526–535. doi:10.1128/EC.4.3.526-535.2005

856 3. Yadav V, Sun S, Heitman J. On the evolution of variation in sexual reproduction through
857 the prism of eukaryotic microbes. Proc Natl Acad Sci USA. 2023;120: e2219120120.
858 doi:10.1073/pnas.2219120120

859 4. Goutte C, Johnson AD. a1 protein alters the dna binding specificity of α2 repressor.
860 Cell. 1988;52: 875–882. doi:10.1016/0092-8674(88)90429-1

861 5. Li T, Stark MR, Johnson AD, Wolberger C. Crystal structure of the MATa1/MATα2
862 homeodomain heterodimer bound to DNA. Science. 1995;270: 262–269.
863 doi:10.1126/science.270.5234.262

864 6. Keleher CA, Goutte C, Johnson AD. The yeast cell-type-specific repressor α2 acts
865 cooperatively with a non-cell-type-specific protein. Cell. 1988;53: 927–936.
866 doi:10.1016/S0092-8674(88)90449-7

867 7. Herskowitz I. A regulatory hierarchy for cell specialization in yeast. Nature. 1989;342:
868 749–757. doi:10.1038/342749a0

869 8. Goutte C, Johnson AD. Yeast a1 and α2 homeodomain proteins form a DNA-binding
870 activity with properties distinct from those of either protein. Journal of Molecular
871 Biology. 1993;233: 359–371. doi:10.1006/jmbi.1993.1517

872 9. Dranginis AM. Binding of yeast a1 and α2 as a heterodimer to the operator DNA of a
873 haploid-specific gene. Nature. 1990;347: 682–685. doi:10.1038/347682a0

874 10. Gillissen B, Bergemann J, Sandmann C, Schroeer B, Bölker M, Kahmann R. A two-
875 component regulatory system for self/non-self recognition in *Ustilago maydis*. Cell.
876 1992;68: 647–657. doi:10.1016/0092-8674(92)90141-X

877 11. Kämper J, Reichmann M, Romeis T, Bölker M, Kahmann R. Multiallelic recognition:
878 Nonself-dependent dimerization of the bE and bW homeodomain proteins in *Ustilago*
879 *maydis*. Cell. 1995;81: 73–83. doi:10.1016/0092-8674(95)90372-0

880 12. Wahl R, Zahiri A, Kämper J. The *Ustilago maydis b* mating type locus controls hyphal
881 proliferation and expression of secreted virulence factors *in planta*. Molecular
882 Microbiology. 2010;75: 208–220. doi:10.1111/j.1365-2958.2009.06984.x

883 13. Vollmeister E, Schipper K, Baumann S, Haag C, Pohlmann T, Stock J, et al. Fungal
884 development of the plant pathogen *Ustilago maydis*. FEMS Microbiol Rev. 2012;36:
885 59–77. doi:10.1111/j.1574-6976.2011.00296.x

886 14. Kües U, Göttgens B, Stratmann R, Richardson WV, O'Shea SF, Casselton LA. A
887 chimeric homeodomain protein causes self-compatibility and constitutive sexual
888 development in the mushroom *Coprinus cinereus*. EMBO J. 1994;13: 4054–4059.
889 doi:10.1002/j.1460-2075.1994.tb06722.x

890 15. Francisco EC, de Jong AW, Hagen F. Cryptococcosis and *Cryptococcus*.
891 Mycopathologia. 2021;186: 729–731. doi:10.1007/s11046-021-00577-7

892 16. Brown GD, Ballou ER, Bates S, Bignell EM, Borman AM, Brand AC, et al. The
893 pathobiology of human fungal infections. Nat Rev Microbiol. 2024;22: 687–704.
894 doi:10.1038/s41579-024-01062-w

895 17. Sun S, Coelho MA, David-Palma M, Priest SJ, Heitman J. The evolution of sexual
896 reproduction and the mating-type Locus: links to pathogenesis of *Cryptococcus*
897 human pathogenic fungi. Annu Rev Genet. 2019;53: 417–444. doi:10.1146/annurev-
898 genet-120116-024755

899 18. Bian Z, Xu Z, Peer A, Choi Y, Priest SJ, Akritidou K, et al. Essential genes encoded by the
900 mating-type locus of the human fungal pathogen *Cryptococcus neoformans*.
901 Genetics; 2024. doi:10.1101/2024.12.02.626420

902 19. Sun S, Coelho MA, David-Palma M, Huang J, Bian Z, Heitman J. Fungal sexual
903 reproduction and mating-type loci. Current Biology. 2025;35: R496–R503.
904 doi:10.1016/j.cub.2025.04.061

905 20. Kwon-Chung KJ, Bennett JE. Distribution of alpha and alpha mating types of
906 *Cryptococcus neoformans* among natural and clinical isolates. American Journal of
907 Epidemiology. 1978;108: 337–340. doi:10.1093/oxfordjournals.aje.a112628

908 21. Yan Z, Hull CM, Heitman J, Sun S, Xu J. *SXI1*α controls uniparental mitochondrial
909 inheritance in *Cryptococcus neoformans*. Current Biology. 2004;14: R743–R744.
910 doi:10.1016/j.cub.2004.09.008

911 22. Hull CM, Davidson RC, Heitman J. Cell identity and sexual development in
912 *Cryptococcus neoformans* are controlled by the mating-type-specific homeodomain
913 protein Sxi1α. Genes Dev. 2002;16: 3046–3060. doi:10.1101/gad.1041402

914 23. Hull CM, Cox GM, Heitman J. The α-specific cell identity factor Sxi1α is not required for
915 virulence of *Cryptococcus neoformans*. Infect Immun. 2004;72: 3643–3645.
916 doi:10.1128/IAI.72.6.3643-3645.2004

917 24. Sun S, Fu C, Ianiri G, Heitman J. The pheromone and pheromone receptor mating-type
918 locus is involved in controlling uniparental mitochondrial inheritance in
919 *Cryptococcus*. Genetics. 2020;214: 703–717. doi:10.1534/genetics.119.302824

920 25. Hsueh Y-P, Fraser JA, Heitman J. Transitions in sexuality: recapitulation of an ancestral
921 tri- and tetrapolar mating system in *Cryptococcus neoformans*. Eukaryot Cell. 2008;7:
922 1847–1855. doi:10.1128/EC.00271-08

923 26. Ekena JL, Stanton BC, Schiebe-Owens JA, Hull CM. Sexual development in
924 *Cryptococcus neoformans* requires *CLP1* , a target of the homeodomain transcription
925 factors Sxi1α and Sxi2**a**. Eukaryot Cell. 2008;7: 49–57. doi:10.1128/EC.00377-07

926 27. Hsueh Y-P, Xue C, Heitman J. A constitutively active GPCR governs morphogenic
927 transitions in *Cryptococcus neoformans*. EMBO J. 2009;28: 1220–1233.
928 doi:10.1038/emboj.2009.68

929 28. Heimel K, Scherer M, Schuler D, Kämper J. The *Ustilago maydis* Clp1 protein
930 orchestrates pheromone and *b* -dependent signaling pathways to coordinate the cell
931 cycle and pathogenic development. The Plant Cell. 2010;22: 2908–2922.
932 doi:10.1105/tpc.110.076265

933 29. Mead ME, Stanton BC, Kruzel EK, Hull CM. Targets of the Sex Inducer homeodomain
934 proteins are required for fungal development and virulence in *Cryptococcus*
935 *neoformans*. Mol Microbiol. 2015;95: 804–818. doi:10.1111/mmi.12898

936 30. Lin X, Hull CM, Heitman J. Sexual reproduction between partners of the same mating
937 type in *Cryptococcus neoformans*. Nature. 2005;434: 1017–1021.
938 doi:10.1038/nature03448

939 31. Sun S, Bian Z, Xu Z, Choi Y, Heitman J. Unisexual reproduction in the global human
940 fungal pathogen *Cryptococcus neoformans*. bioRxiv; 2025.
941 doi:10.1101/2025.06.02.657540

942 32. Sun S, Roth C, Floyd Averette A, Magwene PM, Heitman J. Epistatic genetic
943 interactions govern morphogenesis during sexual reproduction and infection in a
944 global human fungal pathogen. Proc Natl Acad Sci USA. 2022;119: e2122293119.
945 doi:10.1073/pnas.2122293119

946 33. Desjardins CA, Giamberardino C, Sykes SM, Yu C-H, Tenor JL, Chen Y, et al. Population
947 genomics and the evolution of virulence in the fungal pathogen *Cryptococcus*
948 *neoformans*. Genome Res. 2017;27: 1207–1219. doi:10.1101/gr.218727.116

949 34. Hitchcock M, Thorn V, Samarasinghe H, Sun S, Heitman J, Xu J. Genomic evidence for
950 a-α heterothallic and α-α unisexual mating and recombination in an environmental
951 *Cryptococcus deneoformans* population. Wang L, editor. PLoS Genet. 2025;21:
952 e1011844. doi:10.1371/journal.pgen.1011844

953 35. Sun S, Billmyre RB, Mieczkowski PA, Heitman J. Unisexual reproduction drives meiotic
954 recombination and phenotypic and karyotypic plasticity in *Cryptococcus neoformans*.
955 Butler G, editor. PLoS Genet. 2014;10: e1004849. doi:10.1371/journal.pgen.1004849

956 36. Roth C, Sun S, Billmyre RB, Heitman J, Magwene PM. A high-resolution map of meiotic
957 recombination in *Cryptococcus deneoformans* demonstrates decreased
958 recombination in unisexual reproduction. Genetics. 2018;209: 567–578.
959 doi:10.1534/genetics.118.300996

960 37. Zhai B, Zhu P, Foyle D, Upadhyay S, Idnurm A, Lin X. Congenic strains of the
961 filamentous form of *Cryptococcus neoformans* for studies of fungal morphogenesis
962 and virulence. Infect Immun. 2013;81: 2626–2637. doi:10.1128/IAI.00259-13

963 38. Huang MY, Joshi MB, Boucher MJ, Lee S, Loza LC, Gaylord EA, et al. Short homology-
964 directed repair using optimized Cas9 in the pathogen *Cryptococcus neoformans*
965 enables rapid gene deletion and tagging. Genetics. 2022;220: iyab180.
966 doi:10.1093/genetics/iyab180

967 39. Fan Y, Lin X. Multiple applications of a transient CRISPR-Cas9 coupled with
968 electroporation (TRACE) system in the *Cryptococcus neoformans* species complex.
969 Genetics. 2018;208: 1357–1372. doi:10.1534/genetics.117.300656

970 40. Li T. Crystal structure of the MATa1/MATalpha2 homeodomain heterodimer in complex
971 with DNA containing an A-tract. Nucleic Acids Research. 1998;26: 5707–5718.
972 doi:10.1093/nar/26.24.5707

973 41. Casselton LA, Olesnicky NS. Molecular Genetics of Mating Recognition in
974 Basidiomycete Fungi. Microbiol Mol Biol Rev. 1998;62: 55–70.
975 doi:10.1128/MMBR.62.1.55-70.1998

976 42. Passmore S, Maine GT, Elble R, Christ C, Tye BK. *Saccharomyces cerevisiae* protein
977 involved in plasmid maintenance is necessary for mating of MAT alpha cells. J Mol
978 Biol. 1988;204: 593–606. doi:10.1016/0022-2836(88)90358-0

979 43. Elble R, Tye BK. Both activation and repression of a-mating-type-specific genes in
980 yeast require transcription factor Mcm1. Proc Natl Acad Sci U S A. 1991;88: 10966–
981 10970. doi:10.1073/pnas.88.23.10966

982 44. Tan S, Richmond TJ. Crystal structure of the yeast MATα2/MCM1/DNA ternary
983 complex. Nature. 1998;391: 660–666. doi:10.1038/35563

984 45. Huang J, Rowe D, Subedi P, Zhang W, Suelter T, Valent B, et al. CRISPR-Cas12a
985 induced DNA double-strand breaks are repaired by multiple pathways with different
986 mutation profiles in *Magnaporthe oryzae*. Nat Commun. 2022;13: 7168.
987 doi:10.1038/s41467-022-34736-1

988 46. Huang J, Cook DE. The contribution of DNA repair pathways to genome editing and
989 evolution in filamentous pathogens. FEMS Microbiol Rev. 2022;46: fuac035.
990 doi:10.1093/femsre/fuac035

991 47. Xue C, Tada Y, Dong X, Heitman J. The human fungal pathogen *Cryptococcus* can
992 complete its sexual cycle during a pathogenic association with plants. Cell Host &
993 Microbe. 2007;1: 263–273. doi:10.1016/j.chom.2007.05.005

994 48. Phadke SS, Feretzaki M, Heitman J. Unisexual reproduction enhances fungal
995 competitiveness by promoting habitat exploration via hyphal growth and sporulation.
996 Eukaryot Cell. 2013;12: 1155–1159. doi:10.1128/EC.00147-13

997 49. Jung K-W, Yang D-H, Maeng S, Lee K-T, So Y-S, Hong J, et al. Systematic functional
998 profiling of transcription factor networks in *Cryptococcus neoformans*. Nat Commun.
999 2015;6: 6757. doi:10.1038/ncomms7757

1000 50. Peterson PP, Choi J-T, Fu C, Cowen LE, Sun S, Bahn Y-S, et al. The *Cryptococcus*
1001 *neoformans* STRIPAK complex controls genome stability, sexual development, and
1002 virulence. PLoS Pathog. 2024;20: e1012735. doi:10.1371/journal.ppat.1012735

1003 51. Lin X, Jackson JC, Feretzaki M, Xue C, Heitman J. Transcription factors Mat2 and Znf2
1004 operate cellular circuits orchestrating opposite- and same-sex mating in
1005 *Cryptococcus neoformans*. Dutcher SK, editor. PLoS Genet. 2010;6: e1000953.
1006 doi:10.1371/journal.pgen.1000953

1007 52. Liu H, Yao X, Ke W, Ding H, He G-J, Ma S, et al. A velvet transcription factor specifically
1008 activates mating through a novel mating-responsive protein in the human fungal
1009 pathogen *Cryptococcus deneoformans*. Gao B, editor. Microbiol Spectr. 2022;10:
1010 e02653-21. doi:10.1128/spectrum.02653-21

1011 53. Fu C, Heitman J. PRM1 and KAR5 function in cell-cell fusion and karyogamy to drive
1012 distinct bisexual and unisexual cycles in the *Cryptococcus* pathogenic species
1013 complex. PLoS Genet. 2017;13: e1007113. doi:10.1371/journal.pgen.1007113

1014 54. Fu C, Davy A, Holmes S, Sun S, Yadav V, Gusa A, et al. Dynamic genome plasticity
1015 during unisexual reproduction in the human fungal pathogen *Cryptococcus*
1016 *deneoformans*. PLoS Genet. 2021;17: e1009935. doi:10.1371/journal.pgen.1009935

1017 55. Rutherford JC, Lin X, Nielsen K, Heitman J. Amt2 permease is required to induce
1018 ammonium-responsive invasive growth and mating in *Cryptococcus neoformans*.
1019 Eukaryot Cell. 2008;7: 237–246. doi:10.1128/EC.00079-07

1020 56. Gyawali R, Upadhyay S, Way J, Lin X. A family of secretory proteins Is associated with
1021 different morphotypes in *Cryptococcus neoformans*. Schottel JL, editor. Appl Environ
1022 Microbiol. 2017;83: e02967-16. doi:10.1128/AEM.02967-16

1023 57. Coelho MA, David-Palma M, Kachalkin AV, Kolařík M, Turchetti B, Sampaio JP, et al.
1024 Genomic and phenotypic insights into the expanding phylogenetic landscape of the
1025 *Cryptococcus* genus. bioRxiv; 2025. doi:10.1101/2025.06.18.660340

1026 58. Mackie AM, Hassan KA, Paulsen IT, Tetu SG. Biolog phenotype microarrays for
1027 phenotypic characterization of microbial cells. Methods Mol Biol. 2014;1096: 123–
1028 130. doi:10.1007/978-1-62703-712-9_10

1029 59. Cabrita A, David-Palma M, Brito PH, Heitman J, Coelho MA, Gonçalves P. Multiple
1030 pathways to homothallism in closely related yeast lineages in the basidiomycota.
1031 mBio. 2021;12: e03130-20. doi:10.1128/mBio.03130-20

1032 60. David-Palma M, Sampaio JP, Gonçalves P. Genetic dissection of sexual reproduction in
1033 a primary homothallic basidiomycete. PLoS Genet. 2016;12: e1006110.
1034 doi:10.1371/journal.pgen.1006110

1035 61. Gillissen B, Bergemann J, Sandmann C, Schroeer B, Bölker M, Kahmann R. A two-
1036 component regulatory system for self/non-self recognition in Ustilago maydis. Cell.
1037 1992;68: 647–657. doi:10.1016/0092-8674(92)90141-X

1038 62. Zirión-Martínez C, Magwene PM. WeavePop: A bioinformatics workflow to explore and
1039 analyze genomic variants of eukaryotic populations. Gresham D, editor. G3: Genes,
1040 Genomes, Genetics. 2026; jkag039. doi:10.1093/g3journal/jkag039

1041 63. Huang J, Larmore CJ, Priest SJ, Xu Z, Dietrich FS, Yadav V, et al. Distinct evolutionary
1042 trajectories following loss of RNA interference in *Cryptococcus neoformans*. Proc Natl
1043 Acad Sci USA. 2024;121: e2416656121. doi:10.1073/pnas.2416656121

1044 64. Madhani HD, Styles CA, Fink GR. MAP kinases with distinct Inhibitory functions impart
1045 signaling specificity during yeast differentiation. Cell. 1997;91: 673–684.
1046 doi:10.1016/S0092-8674(00)80454-7

1047 65. Abramson J, Adler J, Dunger J, Evans R, Green T, Pritzel A, et al. Accurate structure
1048 prediction of biomolecular interactions with AlphaFold 3. Nature. 2024;630: 493–500.
1049 doi:10.1038/s41586-024-07487-w

1050 66. Meng EC, Goddard TD, Pettersen EF, Couch GS, Pearson ZJ, Morris JH, et al. UCSF
1051 ChimeraX : Tools for structure building and analysis. Protein Science. 2023;32: e4792.
1052 doi:10.1002/pro.4792

1053 67. Gietz D, St Jean A, Woods RA, Schiestl RH. Improved method for high efficiency
1054 transformation of intact yeast cells. Nucleic Acids Res. 1992;20: 1425.
1055 doi:10.1093/nar/20.6.1425

1056 68. Li H, Durbin R. Fast and accurate short read alignment with Burrows–Wheeler
1057 transform. Bioinformatics. 2009;25: 1754–1760. doi:10.1093/bioinformatics/btp324

1058 69. Sun S, Priest SJ, Heitman J. *Cryptococcus neoformans* mating and genetic Crosses.
1059 Current Protocols in Microbiology. 2019;53: e75. doi:10.1002/cpmc.75

1060 70. Tanaka R, Taguchi H, Takeo K, Miyaji M, Nishimura K. Determination of ploidy in
1061 *Cryptococcus neoformans* by flow cytometry. J Med Vet Mycol. 1996;34: 299–301.

1062 71. Chen S. fastp 1.0: An ultra-fast all-round tool for FASTQ data quality control and
1063 preprocessing. iMeta. 2025;4: e70078. doi:10.1002/imt2.70078

1064 72. Dobin A, Davis CA, Schlesinger F, Drenkow J, Zaleski C, Jha S, et al. STAR: ultrafast
1065 universal RNA-seq aligner. Bioinformatics. 2013;29: 15–21.
1066 doi:10.1093/bioinformatics/bts635

1067 73. Liu D. Algorithms for efficiently collapsing reads with Unique Molecular Identifiers.
1068 PeerJ. 2019;7: e8275. doi:10.7717/peerj.8275

1069 74. Wang L, Wang S, Li W. RSeQC: quality control of RNA-seq experiments.
1070 Bioinformatics. 2012;28: 2184–2185. doi:10.1093/bioinformatics/bts356

1071 75. Okonechnikov K, Conesa A, García-Alcalde F. Qualimap 2: advanced multi-sample
1072 quality control for high-throughput sequencing data. Bioinformatics. 2016;32: 292–
1073 294. doi:10.1093/bioinformatics/btv566

1074 76. Ewels P, Magnusson M, Lundin S, Käller M. MultiQC: summarize analysis results for
1075 multiple tools and samples in a single report. Bioinformatics. 2016;32: 3047–3048.
1076 doi:10.1093/bioinformatics/btw354

1077 77. Liao Y, Smyth GK, Shi W. featureCounts: an efficient general purpose program for
1078 assigning sequence reads to genomic features. Bioinformatics. 2014;30: 923–930.
1079 doi:10.1093/bioinformatics/btt656

1080 78. Robinson MD, McCarthy DJ, Smyth GK. edgeR: a Bioconductor package for differential
1081 expression analysis of digital gene expression data. Bioinformatics. 2010;26: 139–140.
1082 doi:10.1093/bioinformatics/btp616

1083 79. Kechin A, Boyarskikh U, Kel A, Filipenko M. cutPrimers: A new tool for accurate cutting
1084 of primers from reads of targeted next generation sequencing. Journal of
1085 Computational Biology. 2017;24: 1138–1143. doi:10.1089/cmb.2017.0096

1086 80. Quinlan AR, Hall IM. BEDTools: a flexible suite of utilities for comparing genomic
1087 features. Bioinformatics. 2010;26: 841–842. doi:10.1093/bioinformatics/btq033

1088 81. Kim D, Paggi JM, Park C, Bennett C, Salzberg SL. Graph-based genome alignment and
1089 genotyping with HISAT2 and HISAT-genotype. Nat Biotechnol. 2019;37: 907–915.
1090 doi:10.1038/s41587-019-0201-4

1091 82. Shumate A, Salzberg SL. Liftoff: accurate mapping of gene annotations.
1092 Bioinformatics. 2021;37: 1639–1643. doi:10.1093/bioinformatics/btaa1016

1093 83. Loftus BJ, Fung E, Roncaglia P, Rowley D, Amedeo P, Bruno D, et al. The genome of the
1094 basidiomycetous yeast and human pathogen *Cryptococcus neoformans*. Science.
1095 2005;307: 1321–1324. doi:10.1126/science.1103773

1096 84. Love MI, Huber W, Anders S. Moderated estimation of fold change and dispersion for
1097 RNA-seq data with DESeq2. Genome Biol. 2014;15: 550. doi:10.1186/s13059-014-
1098 0550-8

1099

1100 **Main Figures**

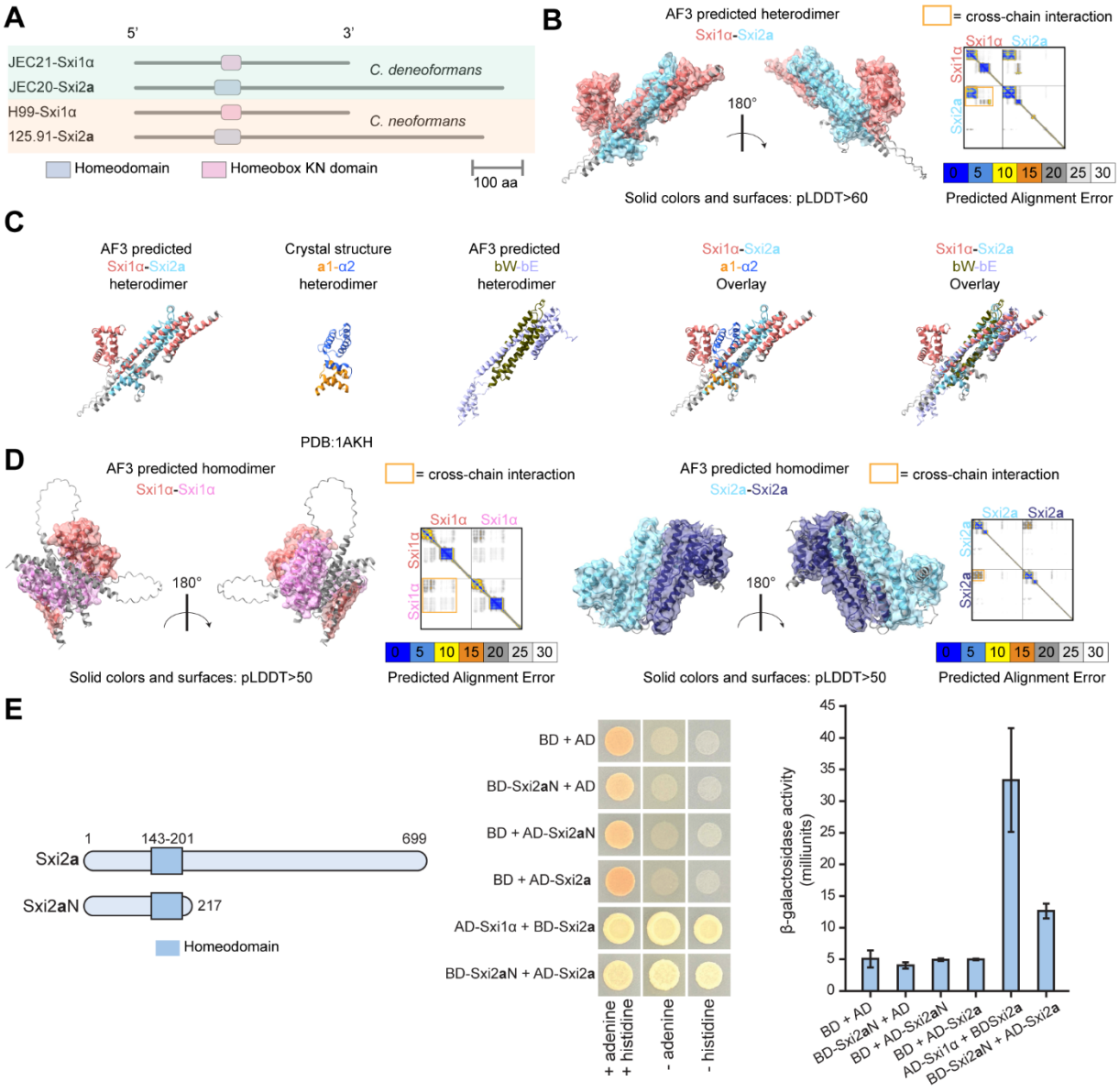

1101

1102 **Figure 1. AlphaFold3 predicts heterodimer and homodimers of Sxi1α and Sxi2a.**

1103 (A) Predicted domain structures of Sxi1α and Sxi2**a** in *C. neoformans* and *C. deneoformans*. (B) AlphaFold3
1104 (AF3)-predicted heterodimer structure of Sxi1α and Sxi2**a** from *C. deneoformans*. C-terminal disordered
1105 regions were hidden for visualization. Only regions with a predicted local distance difference test (pLDDT)
1106 score >60 were colored and surfaced. The predicted alignment error (PAE) plot of the predicted Sxi1α-
1107 Sxi2**a** heterodimer is displayed in the right panel. (C) Overlay of AlphaFold3-predicted Sxi1α-Sxi2**a**
1108 heterodimer with crystal structure of **a**1-α2 (from *S. cerevisiae*, PDB:1AKH) and predicted bW-bE

1109 heterodimer (from *U. maydis*, with high confidence ipTM = 0.74 pTM = 0.64). Pairing was performed with
1110 the "Matchmaker" function in Chimera X. (D) AlphaFold3-predicted homodimer structures with PAE plots
1111 for Sxi1α-Sxi1α (left panel) and Sxi2**a**-Sxi2**a** (right panel). Only regions with a pLDDT score >50 were
1112 colored and surfaced. (E) Yeast two-hybrid analysis of interactions among Sxi1α, Sxi2**a**, and the N terminal
1113 region of Sxi2**a** (Sxi2**a**N). Schematics of Sxi2**a** and Sxi2**a**N constructs are shown on the left, with the
1114 homeodomain indicated. *S. cerevisiae* strains expressing Gal4 DNA-binding domain (BD) or Gal4
1115 activation domain (AD) fusions were mated, and diploids were selected on synthetic dextrose medium.
1116 Protein-protein interactions between bait and prey fusions drive Gal4-dependent activation of *ADE2* and
1117 *HIS3* reporter genes, allowing for growth on medium lacking adenine or histidine. Activation of *ADE2* in the
1118 *ade2* mutant reporter strain background also reduces red pigment accumulation, resulting in lighter colony
1119 coloration on nonselective medium. Quantification of *lacZ* reporter activation was performed using a
1120 chlorophenol red-β-D-galactopyranoside (CPRG) liquid assay, and β-galactosidase activity is shown on the
1121 right. Error bars indicate mean ± standard deviation from three technical replicates.

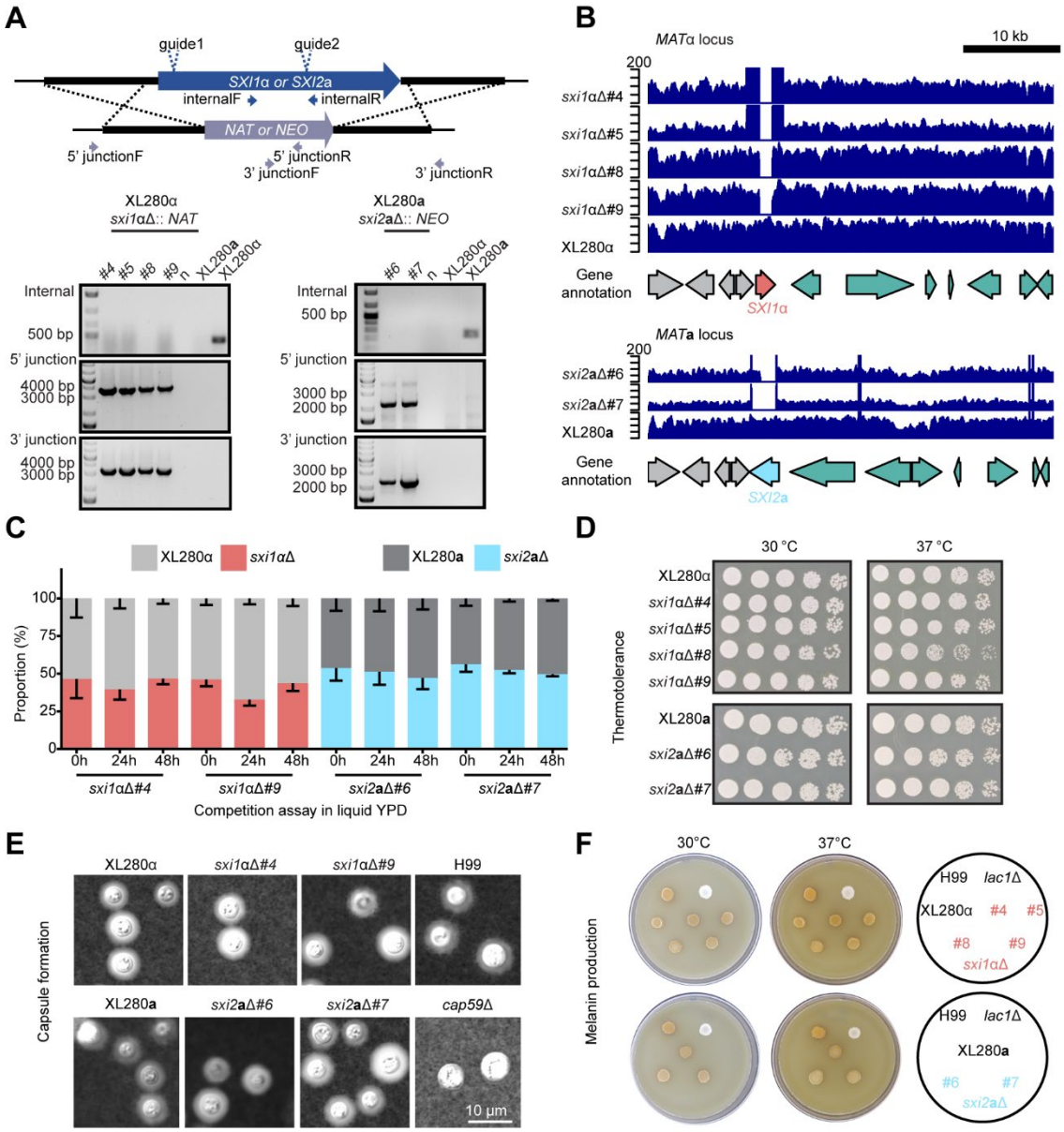

Figure 2. Sxi1α and Sxi2a are not involved in growth, capsule formation, and melanin production. (A) Generation of independent *sxi1*α*Δ* and *sxi2***a***Δ* mutants in XL280α and XL280**a**, respectively. Transformants were verified through internal PCR targeting the ORF, along with 5' and 3' junction PCRs specific to the drug resistance marker to confirm proper integration at the genomic locus. (B) Whole-genome sequencing (WGS) reads mapping confirming the complete or partial deletion of *SXI1*α (red block arrow) and *SXI2***a** (blue block arrow). Genes located within and outside of the mating-type locus are highlighted in green and gray, respectively. (C) *In vitro* competition assays of the *sxi1*α*Δ* and *sxi2***a***Δ* mutants, each carrying either the *NAT* or *NEO* resistance markers, and their corresponding XL280 wildtype strains. Each

1131 competition was assayed after 0, 24, 48 hours of incubation, with four independent replicates. Error bars
1132 indicate standard deviation. (D) Serial dilutions of *sxi1*α*Δ* and *sxi2***a***Δ* mutants, along with the corresponding
1133 XL280 wildtype strains, were spotted on solid YPD media and incubated at 30°C and 37°C. (E) Saturated
1134 cultures of the indicated strains, grown in RPMI medium, were stained with India ink to visualize capsule
1135 formation. The H99 strain and isogenic *cap59*Δ mutant served as positive and negative controls,
1136 respectively. (F) Overnight cultures of the indicated strains were spotted on Niger seed medium to monitor
1137 melanin formation. The wildtype H99 strain and isogenic *lac1*Δ mutant served as positive and negative
1138 controls, respectively.

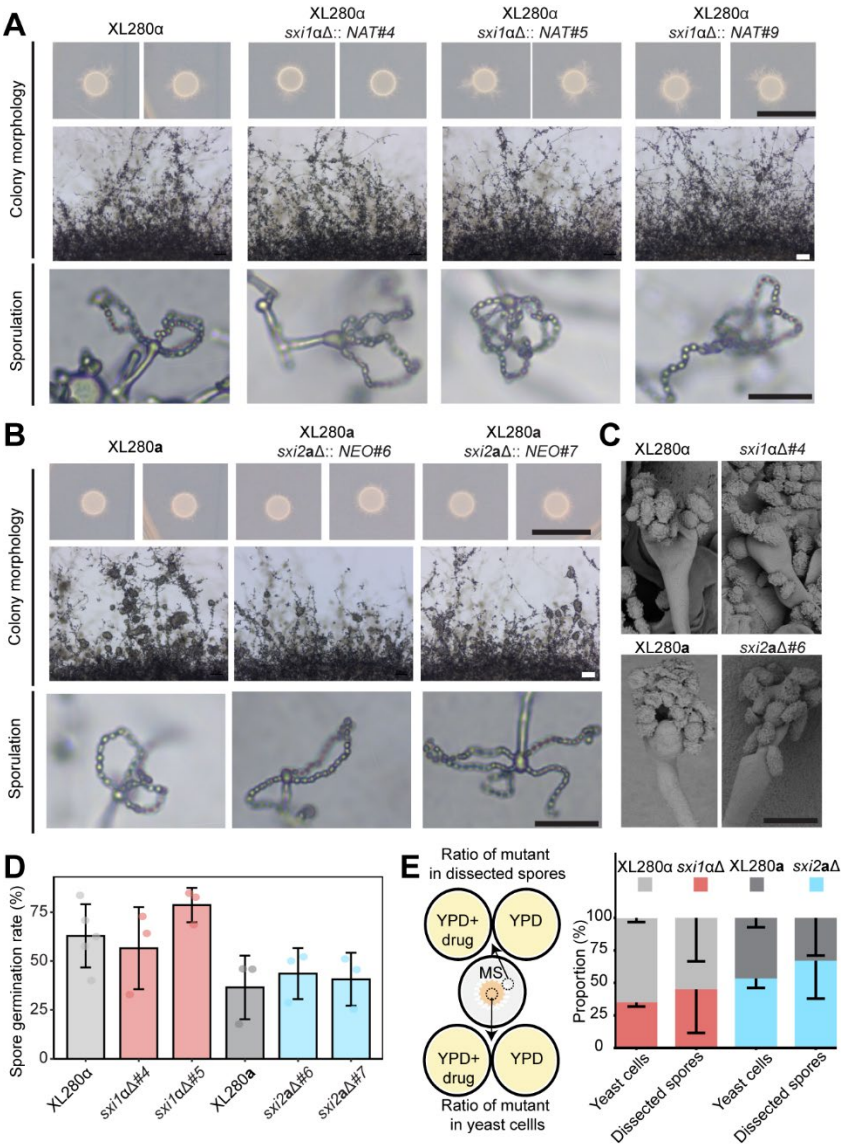

Figure 3. Sxi1α and Sxi2a are not required for hyphal growth or basidium and spore production. (A and B) Colony morphology (top), self-filamentation (middle), and sporulation (bottom) phenotypes of independent *sxi1*αΔ (A) and *sxi2***a**Δ (B) mutants when grown under mating-inducing conditions. Scale bars, 1 cm (upper panel), 100 μm (middle panel) and 20 μm (bottom panel). (C) Scanning electron microscopy (SEM) images of basidia and basidiospores from the indicated solo-culture. Samples were grown on MS media for 1 to 2 weeks before microscopy. Scale bar: 5 μm. (D) Germination rate of random spores dissected from the indicated solo-cultures. At least 3 replicates were performed for each strain (indicated by dots), with error bars depicting standard deviation among replicates. (E) Competition assays of *sxi1*αΔ, *sxi2***a**Δ mutants against their corresponding XL280 wildtype strain. The co-cultures were grown on MS

1149 medium under mating-inducing conditions. Spores from the periphery, and yeast cells from the center, of
1150 the co-culture spots were dissected and analyzed to determine their origin (i.e., wildtype or mutant), which
1151 were then used to infer the relative competitiveness of the mutant strains. Five different co-culture spots
1152 were analyzed for each competition.

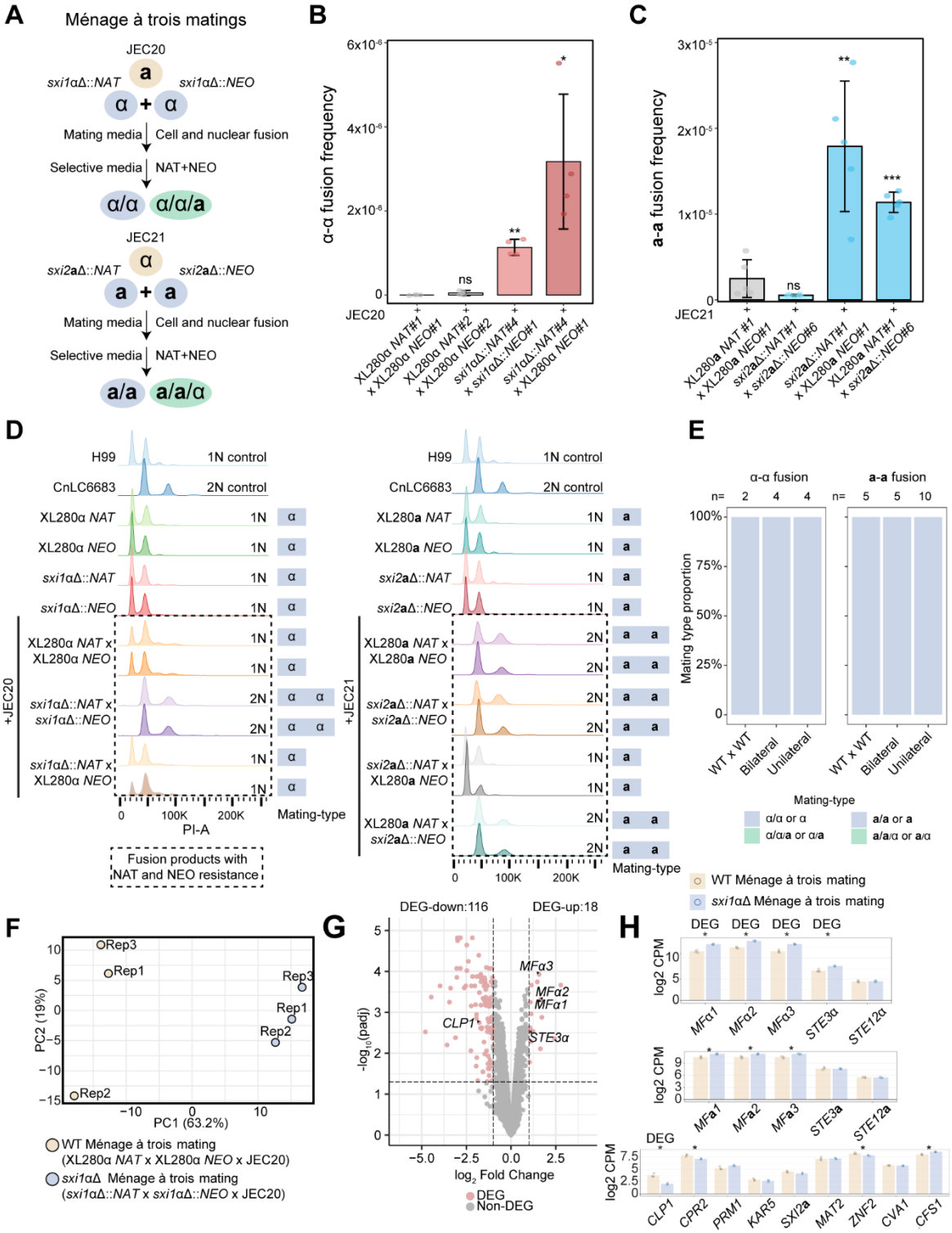

Figure 4. Fusion frequency and ploidy analysis of products from α x α and a x a Ménage à trois matings.

(A) Schematic of the Ménage à trois mating assay. In each mating-type background, two strains carrying different selectable markers (NAT or NEO) were co-cultured with a pheromone donor of the opposite mating

1158 type to induce cell-cell fusion. NAT and NEO resistant colonies were recovered on selective medium. (B-C)
1159 Quantification of α x α (B) and **a** x **a** (C) fusion frequencies for the indicated bilateral and unilateral crosses.
1160 Cells from the indicated mating assay on V8 agar (pH = 7.0) for 72 h were plated on YPD + NAT + NEO
1161 and YPD to determine the ratio of cell-cell fusion products in the population. Data are presented as mean
1162 ± SD from four to five independent biological replicates; each point represents an individual replicate. ns,
1163 not significant; * (p-value < 0.05), ** (p-value < 0.01), *** (p-value < 0.001) indicate statistical significance
1164 compared to wildtype control. (D) Fluorescence-activated cell sorting (FACS) analysis of DNA content in
1165 parental strains and fusion products. H99 (1N control) and CnLC6683 (2N control) originate from the same
1166 experiment; their profiles are duplicated in both the left and right panels to facilitate comparison. Fusion
1167 products (highlighted by dashed boxes) are annotated with their mating type(s) as determined by
1168 genotyping PCR (right). 1N and 2N indicate haploid and diploid DNA content, respectively. (E) Proportion
1169 of mating type of fusion products from the indicated crosses. (F) Principal component analysis (PCA) of 3'
1170 enriched RNA sequencing data from WT (XL280α *NAT* x XL280α *NEO* x JEC20) and *sxi1*αΔ bilateral
1171 (*sxi1*αΔ::*NAT* x *sxi1*αΔ::*NEO* x JEC20) Ménage à trois mating harvested after 72 h on V8 (pH=7) medium.
1172 Each point represents an independent biological replicate. The percentage of variance explained by PC1
1173 and PC2 is indicated. (G) Volcano plot showing differential gene expression between *sxi1*αΔ bilateral and
1174 WT ménage à trois mating. Genes classified as differentially expressed are highlighted in red based on |
1175 $\log_2$ fold change| >=1 and adjusted p-value <= 0.05 thresholds, while non-differentially expressed genes
1176 are shown in gray. Selected genes of interest are labeled. (H) Bar plots showing normalized CPM
1177 expression levels for representative differentially expressed genes DEG and non-differentially expressed
1178 genes across WT and *sxi1*αΔ bilateral ménage à trois mating. Data are presented as mean ± standard
1179 deviation across biological replicates. Asterisks indicate statistically significant differences. Statistical
1180 significance was assessed using two sample Welch t tests on TMM normalized $\log_2$ CPM values for each
1181 gene, with p values adjusted for multiple testing with the Benjamini–Hochberg method. Genes labeled as
1182 DEG correspond to those classified as differentially expressed in the DEG analysis.

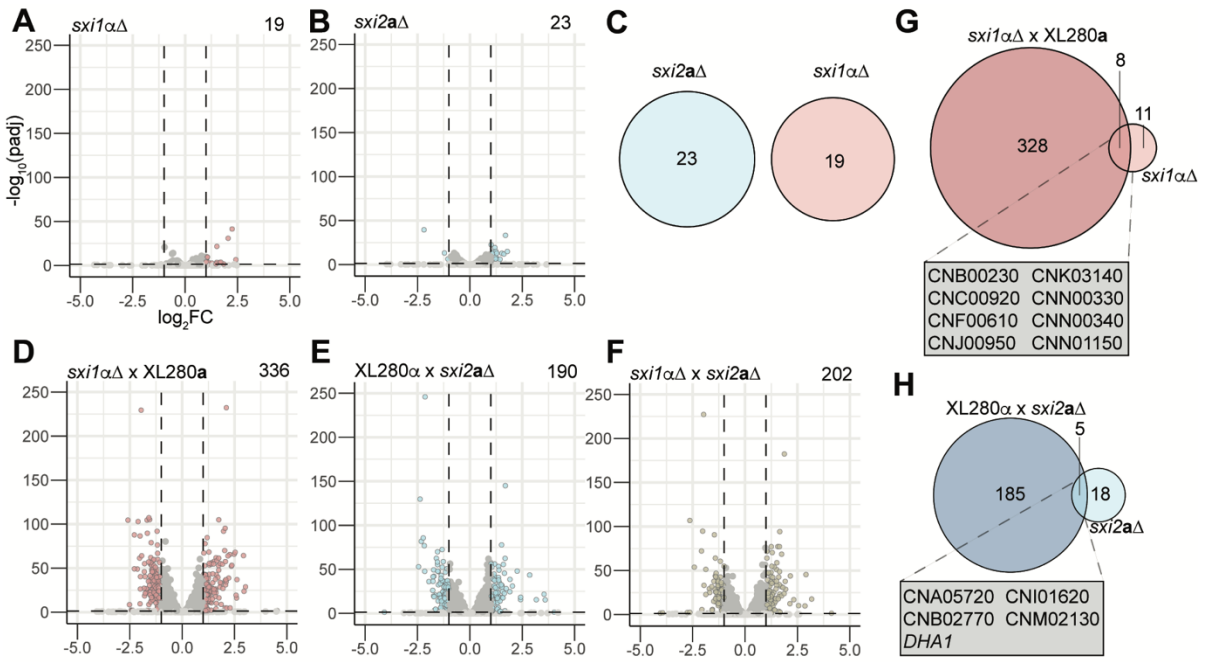

Figure 5. Sxi1α and Sxi2a regulate transcription of distinct subsets of genes during unisexual and bisexual reproduction.

(A and B) Differentially expressed genes in *sxi1*α**Δ** (A) and *sxi2***a**Δ (B) relative to wild-type XL280α or XL280**a**, respectively, during solo cultures (72h at RT on V8 medium). Dashed lines indicate p_{adj} = 0.05 and $\log_2$FC = ± 1. (C) Comparison of DEGs in (A) and (B). (D-F) DEGs relative to XL280α x XL280**a** in crosses between *sxi1*α**Δ** x XL280**a** (D), XL280α x *sxi2***a**Δ (E), and *sxi1*α**Δ** x *sxi2***a**Δ (F). (G and H) Comparisons of DEGs in *sxi1*α**Δ** (G) and *sxi2***a**Δ (H) mutants between solo cultures and α x **a** crosses, with overlapping genes highlighted in the boxes.

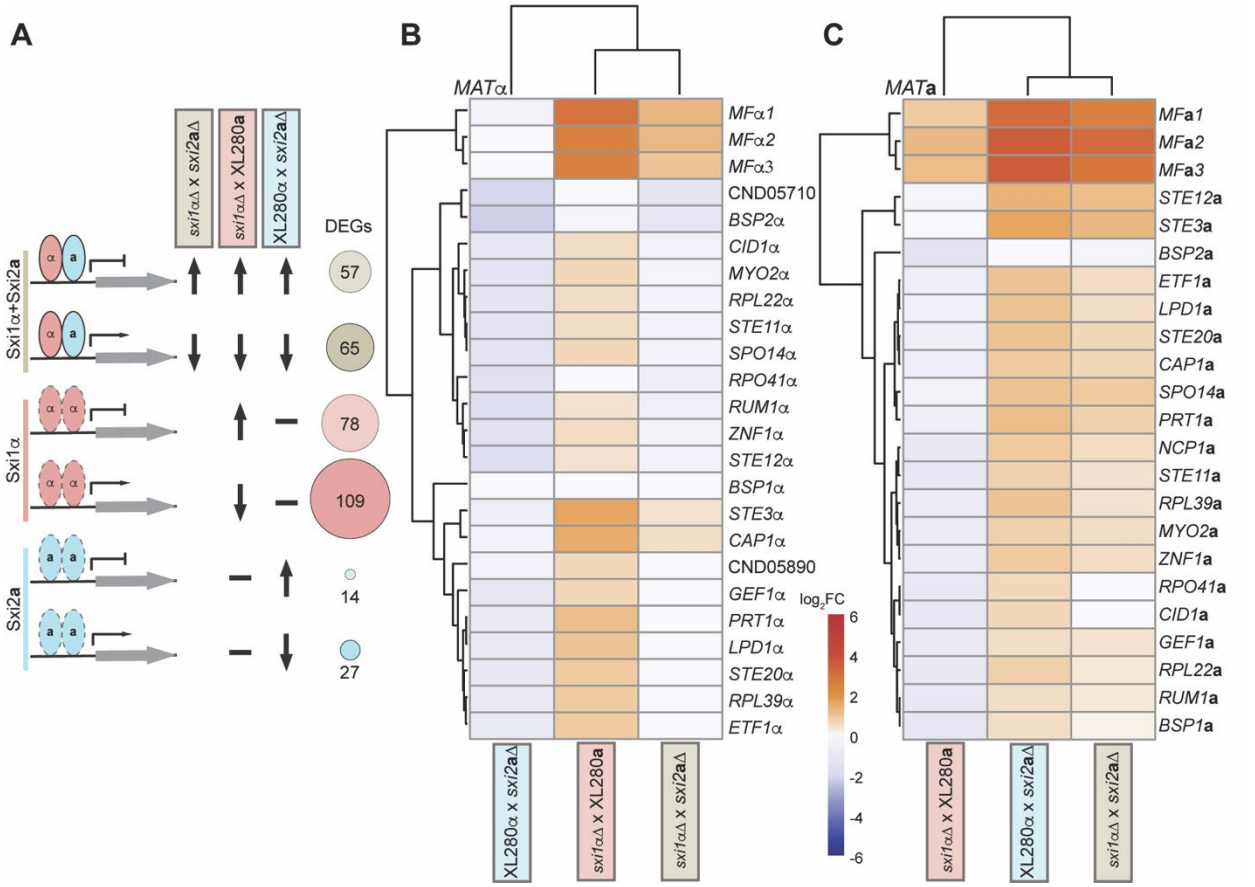

Figure 6. Sxi1α and Sxi2a control mating genes in distinct and opposing manners.

(A) Schematic of 3 hypotheses for Sxi1α and Sxi2**a** function during α x **a** sexual reproduction. Genes in the first scenario are either positively or negatively regulated by the Sxi1α-Sxi2**a** heterodimer and undergo similar expression changes in all crosses lacking functional Sxi1α and/or Sxi2**a**. Genes in the second scenario are regulated by Sxi1α and are differentially expressed in crosses lacking a functional copy of Sxi1α but not in the XL280α x *sxi2***a**Δ cross because expression changes are independent of Sxi2**a**. Genes in the third scenario are differentially expressed in crosses lacking functional Sxi2**a** (XL280α x *sxi2***a**Δ and *sxi1*αΔ x *sxi2***a**Δ) but unchanged in the presence of a functional copy of Sxi2**a** (*sxi1*αΔ x XL280**a**). (B and C) $\log_2$FC expression values of *MAT*α (B) and *MAT***a** (C) genes in *sxi1*αΔ x XL280**a**, XL280α x *sxi2***a**Δ, and *sxi1*αΔ x *sxi2***a**Δ mutant crosses relative to XL280α x XL280**a** wildtype cross.

1203 **Supporting information captions**

1204 Table S1 DEGs identified during Ménage à trois matings.

1205 Table S2 DEGs identified under different mating comparisons.

1206 Table S3 DEGs shard between unisexual and α x **a** sexual reproduction.

1207 Table S4 Strains and plasmids used in this study.

1208 Table S5 Primers used in this study.